



Zachodniopomorski
Uniwersytet
Technologiczny
w Szczecinie

Novel application of large area propeller to optimize Energy Efficiency Design Index (EEDI) of ships

Prabu Duplex

Master Thesis

presented in partial fulfillment
of the requirements for the double degree:
"Advanced Master in Naval Architecture" conferred by University of Liege
"Master of Sciences in Applied Mechanics, specialization in Hydrodynamics,
Energetics and Propulsion" conferred by Ecole Centrale de Nantes

developed at West Pomeranian University of Technology, Szczecin
in the framework of the

"EMSHIP" Erasmus Mundus Master Course in "Integrated Advanced Ship Design"

Ref. 159652-1-2009-1-BE-ERA MUNDUS-EMMC

Supervisor: Prof. Zbigniew Sekulski, West Pomeranian University of
Technology, Szczecin.

Reviewer: Prof. Mihaela Amoraritei, "Dunarea de Jos" University of Galati.

Szczecin, February 2015



Universität
Rostock



Traditio et Innovatio



Zachodniopomorski
Uniwersytet Technologiczny
w Szczecinie



THIS PAGE IS LEFT INTENTIONALLY BLANK

Contents

2	INTRODUCTION.....	11
2.1	Consequences of global warming	11
2.2	Shipping industry and global warming.....	11
2.3	Projected growth of CO ₂ emissions	12
2.4	CO ₂ emissions regulations	12
3	DEVELOPMENT OF EMISSION INDEX AT IMO.....	13
3.1	Energy Efficiency Design Index (EEDI).....	14
3.2	Ship Energy Efficiency Management Plan (SEEMP).....	14
3.3	Energy Efficiency Operational Indicator (EEOI)	15
3.3.1	<i>Application of the efficiency metrics</i>	<i>15</i>
3.3.2	<i>Energy Efficiency Design Index (IMO MEPC resolution 212(63), Annex 8)</i>	<i>16</i>
3.3.3	<i>Application and method of calculation.....</i>	<i>19</i>
3.3.4	<i>Reduction factors and implementation</i>	<i>20</i>
3.3.5	<i>Benefits</i>	<i>20</i>
3.3.6	<i>Emission control measures other than CO₂ (IMO,EU and Class).....</i>	<i>20</i>
3.4	Energy efficiency methods	22
3.4.1	<i>Optimization approach.....</i>	<i>22</i>
3.4.2	<i>Energy saving devices</i>	<i>23</i>
3.4.3	<i>Propulsion improvement / Retrofit solutions working principle</i>	<i>23</i>
3.4.4	<i>Compatibility study.....</i>	<i>25</i>
3.4.5	<i>Structural optimization and light weight construction</i>	<i>26</i>
3.4.6	<i>Machinery technology Waste heat recovery</i>	<i>26</i>
3.4.7	<i>Success stories.....</i>	<i>27</i>
4	MODELING FLUID FLOW.....	28
4.1	Incompressible Navier -Stokes Equations	28
4.2	Reynolds averaged equations.....	29
4.3	Turbulence modeling	30
4.3.1	<i>Zero equation models</i>	<i>30</i>
4.3.2	<i>One equation models</i>	<i>31</i>
4.3.3	<i>Two equation models.....</i>	<i>31</i>
4.3.4	<i>Reynold's stress models</i>	<i>31</i>
4.4	Wall region	32

4.5	Brief introduction of various solution methods in Star-CCM+	33
4.5.1	<i>Finite Volume Method</i>	33
4.5.2	<i>Velocity pressure coupling & basic principle of SIMPLE algorithm:</i>	33
4.5.3	<i>Mesh generation</i>	34
4.5.4	<i>Volume of fluid method</i>	35
4.5.5	<i>Simulating rotation</i>	36
4.5.6	<i>Simulation of flow with rotating geometries</i>	38
4.5.7	<i>Scaling laws</i>	39
5	WORK FLOW ANALYSIS.....	40
5.1	Numerical setup:	40
6	RESISTANCE TEST.....	41
6.1	Setup and test procedure.....	41
6.1.1	<i>Expression of the resistance:</i>	41
6.1.2	<i>ITTC 57 method</i>	42
6.1.3	<i>ITTC 78 method</i>	42
6.2	Experiments	43
6.3	Resistance test Star- CCM+.....	44
6.3.1	<i>Creation of computational domain</i>	44
6.3.2	<i>Generating the volume mesh</i>	44
6.3.3	<i>Grid convergence study (Fn 0.22)</i>	48
6.3.4	<i>EFD vs CFD comparison for resistance and motion</i>	48
6.3.5	<i>Effect of turbulence model on results</i>	49
6.3.6	<i>Residuals and convergence analysis</i>	50
6.3.7	<i>Wave profile</i>	50
6.3.8	<i>Wave profile at service speed</i>	51
6.3.9	<i>Results obtained from mesh1</i>	51
6.3.10	<i>Wake field predicted with various mesh and models</i>	51
7	OPEN WATER TEST	53
7.1	Setup and test procedure.....	53
8	OPEN WATER TEST STAR-CCM+.....	55
8.1	Procedure.....	55
8.1.1	<i>Meshing</i>	55
8.1.2	<i>Experimental setup</i>	56
8.1.3	<i>Methodology</i>	57
8.2	Results	58

9	SELF PROPULSION TEST	59
9.1	Procedure.....	59
9.1.1	<i>Towing force</i>	59
9.1.2	<i>Constant speed or British method</i>	60
9.2	ITTC Recommended practice (2008b) for single screw ships.....	61
9.2.1	<i>Thrust and torque coefficients</i>	61
9.2.2	<i>wake fraction (w)</i>	62
9.2.3	<i>Rotative efficiency</i>	62
9.2.4	<i>Hull efficiency</i>	62
9.2.5	<i>Open water efficiency</i>	62
9.2.6	<i>propulsive efficiency</i>	62
9.3	Self propulsion experiments at CTO S.A	63
10	SELF PROPULSION TESTS STAR-CCM+.....	64
10.1	Introduction	64
10.2	Procedure.....	64
10.2.1	<i>The computational model</i>	64
10.2.2	<i>Mesh1 (Propeller)</i>	65
10.2.3	<i>Mesh2 (Domain and hull)</i>	66
10.2.4	<i>Boundary definition</i>	67
10.2.5	<i>Defining VOF wave and initial condition</i>	67
10.2.6	<i>Selecting the Physics Models</i>	67
10.2.7	<i>Setting solver parameters and stopping criteria</i>	67
10.2.8	<i>External towing force</i>	68
10.2.9	<i>Convergence analysis</i>	68
10.3	Analysis	69
10.4	Results	70
11	PROPELLER RELOCATION	71
11.1	Case 1	71
11.2	Case 2.....	73
11.3	Analysis	74
11.3.1	<i>Thrust deduction and wake fraction</i>	74
11.3.2	<i>Hull efficiency and total resistance</i>	75
11.3.3	<i>Rotative and open water efficiency</i>	77
11.3.4	<i>Propulsive efficiency and delivered power</i>	78
11.3.5	<i>Velocity vector</i>	79

12	APPLICATION	80
13	CONCLUSION	81
14	FUTURE WORK.....	82
15	ACKNOWLEDGEMENTS	83
16	REFERENCES	84
16.1	Publications	84
16.2	MEPC Guidelines	85
16.3	ITTC Procedures	86
16.4	Master thesis	86
16.5	Presentation/ Symposium	86
16.6	Literature	87

Table of figures

Figure 1: CO ₂ Emission from industry (Buhang et al., April 2009).....	11
Figure 2: CO ₂ emissions 2007-2012 (Third IMO GHG Study 2014).....	12
Figure 3: IMO Timeline (31)	13
Figure 4: Baseline Establishment (31).....	16
Figure 5: Reduction in phases (31).....	20
Figure 6: SO _x and NO _x emission limit in ECA.....	21
Figure 7: Compatibility study of energy saving devices (MAN B&W presentation)	25
Figure 8: Vortex behind aircraft, turbulence on the Sun and chemical reactions	29
Figure 9: Prandtl's mixing length l (40).....	30
Figure 10: Velocity profile in logarithmic region[36]	32
Figure 11: Iterative solution method for a coupled simulation of flow. (Morch et al. 2008)	33
Figure 12: Different cell types, From left to right: Tetrahedral, hexahedral, polyhedral and prism.[27]	34
Figure 13: Grids unsuitable(L) and suitable (R) for 2phase flows in VOF model (CD-Adapco 2011) 35	35
Figure 14: Rotating coordinate system in a moving reference frame [28]	37
Figure 15: Sliding mesh between two domains with relative motions [28].....	38
Figure 16: Resistance test experimental setup (47)	41
Figure 17: Fluid domain	44
Figure 18: Volumetric refinement created for waves	45
Figure 19: fig (L) section at water line fig (R) Surface mesh refinement at aft	46
Figure 20: Froude number vs Resistance.....	48
Figure 21 Fig (L) Froude number vs sinkage, fig (R): Froude number vs Total resistance	49
Figure 22: Fig (L) Residuals, Fig (R) Wall Y+ values	50
Figure 23: Monitor plot	50
Figure 24: Wave profile Fig (L) Mesh 1, fig (c) Mesh2, fig (R)Mesh3	51
Figure 25: Wave profile for Fn 0.2433, 0.2654, 0.2875, 0.3096 respectively from left	51
Figure 26: RSM Model (Top), Experiment results (Middle), K- ϵ Mesh 1(Bottom)	52
Figure 27: Experimental set up open water test (47)	53
Figure 28: Open water characteristics of propeller1.....	54
Figure 29: Computational domain.....	55
Figure 30: Mesh refinement and Wall Y+ values	56
Figure 31: Residuals for propeller 1	57
Figure 32: Propeller performance EFD vs CFD.....	58
Figure 33: Experimental setup for self propulsion test (British method) (47)	61
Figure 34: Fig (L): Computational domain Fig (R) Sliding interface around propeller	64
Figure 35: (Mesh in propeller region)	65
Figure 36: Fig (L) & Fig (R) Mesh refinement in various zones	66
Figure 37: Monitor plots Fig (L) Resistance, Fig (R) Torque.....	68
Figure 38: Fig (L) Thrust monitor plot, Fig (R) Residuals	68
Figure 39: Example of thrust identity method	70
Figure 40: Fig (L)Position 0, Fig (C) Position 1, Fig (R) Position 2.....	71
Figure 41: RPS vs SFC behavior.....	72

Figure 42: Fig (L)Position 0, Fig (C) Position 1, Fig (R) Position 2.....	73
Figure 43: Fig (L) Position vs Thrust deduction, (Fig R) Position vs Wake fraction.....	74
Figure 44: (Fig L) Position vs Hull efficiency, (Fig R)Position vs Total resistance	75
Figure 45: Pressure on the hull (Top) Position 0 (Bottom) Position 2.	75
Figure 46: Velocity just upstream of the propeller in a line along y axis.	76
Figure 47: Velocity profile just upstream of the propeller plane (T) Pos 0, (B) Pos 2.....	76
Figure 48: Position vs Rotative efficiency (L), Position vs open water efficiency (R)	77
Figure 49: Position vs Propulsive efficiency (L) Position vs Delivered power (R)	78
Figure 50: Velocity vector just upstream of propeller1 plane (Top) Position 0 (Bottom) Position 2 ..	79
Figure 51: EEDI reduction in various phases	80
Figure 52: Variation of delivered power when propeller moved aft (42).	82
Figure 53: Influence of P/D ratio in propeller design (42)	82

DECLARATION OF AUTHORSHIP

I Prabu Duplex declare that this thesis and the work presented in it are my own and have been generated by me as the result of my own original research.

"Novel application of large area propeller to optimize Energy Efficiency Design Index of ships (EEDI)",

Where I have consulted the published work of others, this is always clearly attributed.

Where I have quoted from the work of others, the source is always given. With the exception of such quotations, this thesis is entirely my own work.

I have acknowledged all main sources of help.

Where the thesis is based on work done by myself jointly with others, I have made clear exactly what was done by others and what I have contributed myself.

This thesis contains no material that has been submitted previously, in whole or in part, for the award of any other academic degree or diploma.

I cede copyright of the thesis in favour of the West Pomeranian University of Technology, Szczecin, Poland.

Date: 17.01.2015



Signature

ABSTRACT

Environmental pollution and rising cost of fossil fuels are posing a major threat to the shipping industry. After globalization its contribution is significant and time has come to curb the emissions from ships. The reduction of CO₂ emissions has been the key target since IMO's Marine Environment Protection Committee (MEPC) published its findings in 2009. A number of measures resulting in technical and operational reductions were made mandatory in 2011. Among these and nearly all new build ships (20) have to conform is Energy Efficiency Design Index (EEDI). This provides a method of establishing the minimum efficiency of new ships depending on the type and size. With increasing competition the key to survival will be to design and operate the ships efficiently. In the current phase designers relied to retrofit methods and achieved slight gains of hull efficiency. In later phases tougher restrictions will be imposed which needs more changes in ship design. The EEDI has become an important design parameter that has to be complied.

This master thesis is a holistic approach to analyze possible methods and implement one in the form of large area propeller as demonstrated in the R&D project Streamline initiated by the seventh frame work of European commission.

Increasing the propeller diameter together with low rotational speed reduces axial and rotational losses (41) there by propulsive efficiency can be improved. But the constraints in the form of hull and ship baseline restrict this. Much research have been done so far by increasing the propeller diameter in the original position and in this work the large area propeller is moved axially aftwards to two positions between the initial location and transom where there was ample space to install it. This resulted in a partial success which will be explained at the end of this thesis. However apart from improved propulsive efficiency, improvement of other factors such as hull efficiency, suction on the hull and wake profile have been gained. The increased clearance reduces the pressure pulses transferred to the hull.

An extensive analysis is made by means of a sliding grid approach in the RANSE CFD code Star-CCM+, with a series of self propulsion tests, for the chosen locations and propellers by moving it systematically aft. Results were validated with the experimental data from Ship Design and Research Centre (Centrum Techniki Okrętowej S.A., Gdańsk, Poland - CTO S.A.). These tests are a starting point of the experiments targeted to achieve the desired efficiency by choosing the optimum Pitch-Diameter ratio (P/D ratio) of the propeller.

1 INTRODUCTION

Melting glaciers, rising sea levels, depleting forests and reducing wildlife are the evident of climate change. These climate change according to IPCC ([Pachauri and Reisinger 2007](#)), are mainly due to the human activities such as deforestation and burning fossil fuels which increase the concentration of green house gases. Excessive green house gas CO_2 in the air makes the green house effect stronger ([EPA](#)) and in turn rises the average temperature of earth's atmosphere and oceans causing global warming and related consequences.

1.1 Consequences of global warming

According to the facts and figures by IPCC plants and animal species are at increased risk of extinction if increase in global average temperature exceeds 1.5-2.5 degrees. Crop productivity will decrease above 3 degrees increase in global temperature above average. This may lead to rise in sea levels and floods. The report also finds that if planet earth continues to get warmer its impact is going to be enormous and five broad categories such as water, ecosystem, food, coasts and health.

1.2 Shipping industry and global warming

Shipping industry is one of the contributor of the green house gases and thus plays a part in global warming. According to IMO's second greenhouse gas ([Buhang et al., April 2009](#)) study shipping is measured to have emitted 1046 million tons of CO_2 during 2007. Emissions of CO_2 from shipping as compared with global CO_2 emissions from other sectors are shown in figure1.

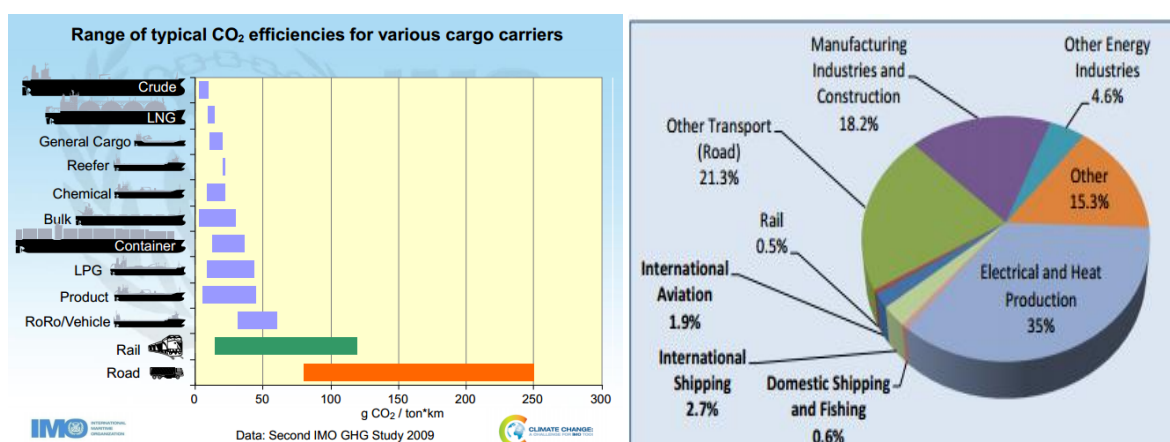


Figure 1: CO₂Emission from industry ([Buhang et al., April 2009](#))

Even though CO₂ emissions from ships accounts for 3% of the global emissions it is by far most efficient mode of commercial transport as a cargo vessel of <8000DWT emits only 15 grams of CO₂ per tonne-km comparing 50g/t-km of heavy truck and 540 g/t-km of airfreight.

1.3 Projected growth of CO₂ emissions

Marine transport's global carbon foot print is projected to grow due to the heavy reliance of ships on oil for propulsion and the expected growth in the world trade driven by expanding global population, world economy and demand for shipping services.

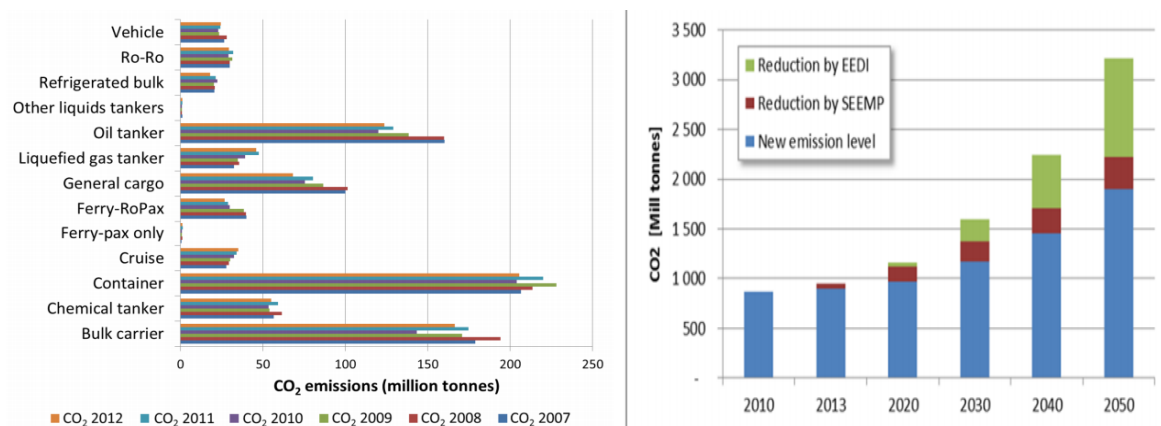


Figure 2: CO₂ emissions 2007-2012 ([Third IMO GHG Study 2014](#))

According to IMO's findings in the absence of policies as a result of the growth in shipping CO₂ emissions from international shipping may grow by a factor of 2-3 as compared to the emissions of 2007 which is projected as 12-18% of global total emissions in 2050 ([Heitmann and Khalilian 2011](#)). It also states that without any policies being enforced this will lie between 6-22% (925-1058Mt of CO₂ emissions) higher in 2020 than that of 2007.

1.4 CO₂ emissions regulations

There are various methods to curb the emissions but it remained the question of authority to implement the rules because shipping is an international trade. The Kyoto Protocol of United Nations on Climate Change (UNFCCC) which aims at fighting global warming does not apply to international shipping because of its global nature. Kyoto protocol acknowledged a need for collaborative action needed to address this issue. Only such an agency which can regulate the entire shipping is IMO ([ICS report, 2014](#)). IMO's Marine Environment Protection Committee considered a range of measures aimed at reducing emissions of GHG from international shipping, including technical, operational and market based measures.

2 DEVELOPMENT OF EMISSION INDEX AT IMO

IMO started working on the development of emission control index and during several meetings of MEPC, the progress was discussed and decisions were made. Finally on the 62nd MEPC session new regulation was adopted which was the first global CO₂ emission control index in the industry [38].

In July 2005, the MEPC at its 53rd session approved interim guidelines for voluntary CO₂ emission indexing for use in trials for the purpose of developing a simple system that could be used voluntarily by ship operators during a trial period.

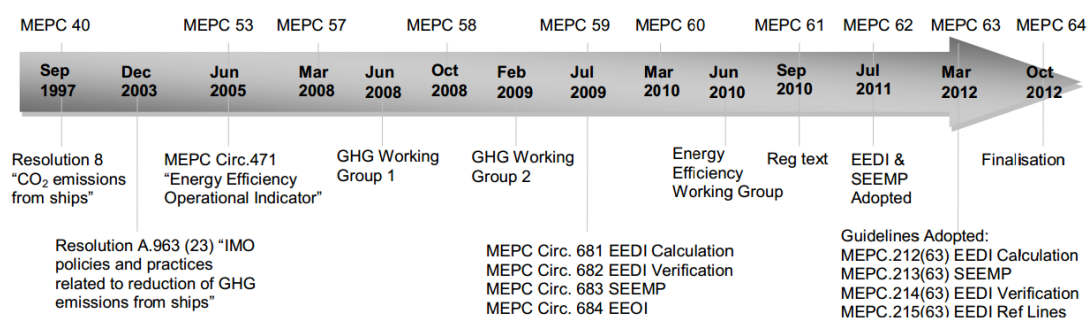


Figure 3: IMO Timeline (31)

MEPC continued their efforts addressing the phenomena of climate change and global warming and in line with the mandate of Kyoto protocol. On its 58th session in October 2008 an energy efficiency design index for new ships and an energy efficiency operational index a management plan suitable for all ships and a voluntary code on best practice in energy efficiency ship operations are developed.

On 59th MEPC meeting in July 2009 it was agreed to spread the following measures and intend to be used for trial purposes until MEPC's 60th session in March 2010.

- Interim guideline on the method of calculation and voluntary verification of Energy Efficiency Design Index (EEDI) for new ships.
- Guidance on the development of a ship Energy Efficiency Management Plan (SEEMP), as well as the guidelines for voluntary use of Ship Energy Efficiency Operational Index (EEOI) for new and existing ships.

On March 2010 during the 60th MEPC meeting the committee has agreed to establish an international work group to work on the EEDI, SEEMP and EEOI. Despite of being capable

of preparing the draft text on mandatory requirements for these regulations it was discussed to sort out the issues concerning ship size, capacity, vessel speed reduction, target dates to implement in relation to the EEDI requirements and an expert group was set up.

On the 61st session all the three indexes were formulated in an applicable form. But the decision to adopt these measures as mandatory under MARPOL Annex VI was planned for the next session.

It was the 62nd session in July 2011 when mandatory measures to reduce emissions of greenhouse gases (GHGs) from international shipping were adopted by parties to MARPOL Annex VI represented in the MEPC.

The amendments to MARPOL Annex VI regulations for the prevention of air pollution from ships add a new chapter 4 to Annex VI on regulations on energy efficiency for ships to make mandatory the Energy Efficiency Design Index (EEDI) for new ships and the Ship Energy Efficiency Management Plan (SEEMP) for all ships. Other amendments to Annex VI add new definitions and the requirements for survey and certification including the format for the International Energy Efficiency Certificate.

2.1 Energy Efficiency Design Index (EEDI)

The EEDI was formally adopted by the IMO in July 2011 and applies to new ships built from 2013 onwards. The EEDI can be considered as a performance based tool that allows ship designers and builders to choose from various available cost effective technologies that can be used for a specific ship design. The EEDI provides a specific figure for an individual ship design expressed in grams of CO₂ per ship's capacity mile (smaller value indicates better efficiency). The formulation takes in to account ship's emissions, capacity and speed. There is a reference value and the attained EEDI value should be less than this.

2.2 Ship Energy Efficiency Management Plan (SEEMP)

The purpose of SEEMP is to establish a mechanism for a company and specific ship to improve the energy efficiency of ship's operation (21). IMO requirements, industry initiatives, fuel prices and corporate responsibility are driving owners/operators to implement a Ship Energy Efficiency Management Plan (SEEMP). In July 2011, IMO adopted an amendment to MARPOL Annex VI that makes SEEMP mandatory for all new and existing ships as of 1 January 2013. The scope and detail of SEEMP can vary and there are several

guidelines already published for owners and operators to reference. It is also to be mentioned that the best package of measures for a ship to improve efficiency differs from ship type, cargo, route and other factors as mentioned in MEPC 1/683. SEEMP is implemented in planning, implementation, monitoring, and Self evaluated improvement stage.

2.3 Energy Efficiency Operational Indicator (EEOI)

The IMO has also developed the Energy Efficiency Operational Indicator (EEOI), an indicator that provides information concerning the efficiency of the ship in operations (22). The calculation is based on individual vessel's fuel consumption and data on the achieved transport work (e.g. cargo, mass, number of passengers etc) resulting in a figure of CO₂ emissions per ton nautical mile. The full EEOI equation is contained in the circular letter MEPC.1/Circ.684 and can be summarised as

$$EEOI = \frac{\text{Fuel consumption} \cdot \text{Carbon conversion}}{\text{Distance sailed} \cdot \text{Cargo transported}}$$

Unlike the EEDI, the EEOI is not limited to new vessels and can be used to measure the real efficiency of a ship in operation and to gauge the effects of any changes such as hull and propeller cleaning, slow steaming, improved voyage planning etc. The EEOI can be improved by increasing the amount of cargo transported or by applying any measure aiming at reducing the fuel consumption (eg: slow steaming, vessel modifications, weather routing etc). As this formulation depends on ship activities and operations it will vary over time and voyages.

2.3.1 Application of the efficiency metrics

During MEPC 63 some parties took a strong opposition against the application of the EEDI formula for existing ships and this view was endorsed by the committee however it has been implemented and new ship categories added over years. The application of the EEOI remains non mandatory but it has been included in the ship Energy Efficiency Management Plan (SEEMP) as a possible index to verify and measure its effectiveness. While the IMO decided not to use the EEOI indicator as a basis for regulation.

2.3.2 Energy Efficiency Design Index (IMO MEPC resolution 212(63), Annex 8)

2.3.2.1 Base line formulation

EEDI formula calculates the CO₂ emission efficiency of a vessel at the design stage in terms of (gCO₂/tonne-nm). In order to implement CO₂ emission regulations stepwise making emission criteria rigorous over time IMO first developed the EEDI baseline from the data collected from existing ships using Lloyds fair play (LRFP) database. These baselines are developed for each category of ship like bulk carrier, container etc. The EEDI reference line refer to the statistically averaged EEDI curves derived from data for existing ships.

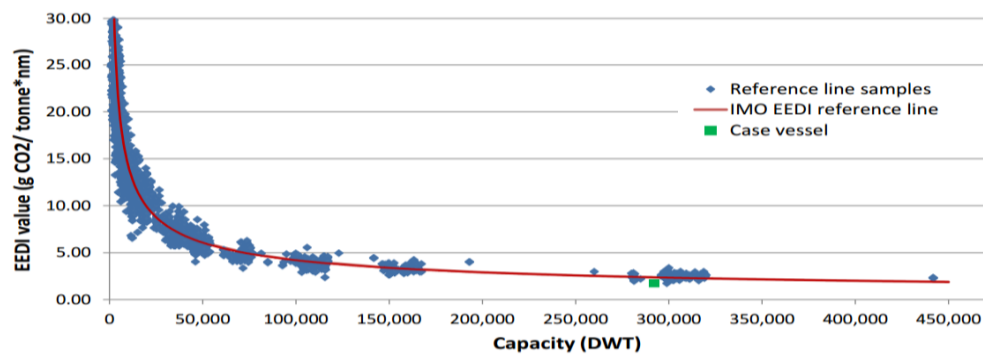


Figure 4: Baseline Establishment (31)

2.3.2.2 The formula

The basic of creating the index is to represent CO₂ efficiency of ship at design point. The simplest way to represent the EEDI formula is

$$EEDI = \frac{CO_2 \text{ Emission}}{\text{Transport work}}$$

The source of the CO₂ emissions from the ship comprises of emission from the main engine, auxilliary engine at certain power defined by the ship's operating speed. Transport work is the product of ship capacity (DWT) and speed (V_{ref}). So again we can rewrite the formula as,

$$EEDI = \frac{CO_{2ME} + CO_{2AE}}{\text{Capacity} \times V_{ref}}$$

The main and auxiliary engine emissions can be calculated by multiplying fuel consumption of the main and auxiliary engines with the carbon conversion factor (C_f), which connects the fuel consumption to the amount of CO₂ emissions. Thus the formula can be written as,

$$EEDI = \frac{(FC_{ME} \times C_{FME}) + (FC_{AE} \times C_{FAE})}{\text{Capacity} \times V_{ref}}$$

Fuel consumption of an engine can be calculated as a product of produced power (P) and Specific fuel consumption (SFC). So again,

$$EEDI = \frac{(P_{ME} \times SFC_{ME} \times C_{FME}) + (P_{AE} \times SFC_{AE} \times C_{FAE})}{Capacity \times V_{ref}}$$

Some ships are fitted with energy saving technologies like waste heat recovery system, sails, solar panels etc which reduce the power required either from main and auxilliary engines (P_{eff} and P_{AEeff}).

Power take in electrical motors (P_{PTI}) on propeller shaft are installed in some ships and the impact of these devices are also included. These factors are taken care in the formula by subtracting the emission reduction due to innovative technologies. Thus the formula can be written as,

$$EEDI = \frac{(P_{ME} \times SFC_{ME} \times C_{FME}) + (P_{AE} \times SFC_{AE} \times C_{FAE}) + ((P_{PTI} - P_{AEeff}) \times SFC_{AE} \times C_{FAE}) - (P_{eff} \times SFC_{AE} \times C_{FME})}{Capacity \times V_{ref}}$$

Some ships with special design elements may require additional installed main power (ice class ships). This is taken care of by introducing a power correction factor (f_j) which normalises the installed main engine power. A capacity correction factor (f_i) is included in the formula because capacity of the ship may be limited due to technical or regulatory reasons. A weather correction coefficient (f_w) is included to normalise the speed of the ship as ships are designed for various operation conditions of wave height, wave frequency and wind speed. A cubic correction factor (f_c) is included to normalise the capacity for chemical tankers and gas carriers. When these non dimensional factors are included the formula becomes for taking into consideration multiple engines and factors,

$$\begin{aligned} & \frac{f_j (P_{ME} \times SFC_{ME} \times C_{FME}) + (P_{AE} \times SFC_{AE} \times C_{FAE}) + ((f_j \cdot P_{PTI} - P_{AEeff}) \times SFC_{AE} \times C_{FAE}) - (P_{eff} \times SFC_{AE} \times C_{FME})}{f_i \times f_c \times Capacity \times V_{ref} \times f_w} \\ & = \frac{kW * \frac{g_{fuel}}{kWh} * \frac{g_{CO2}}{g_{fuel}}}{Tonne * knotal\ mile/h} = \frac{g_{CO2}}{Tonne * knotal\ mile} \end{aligned}$$

$$\left[\left(\prod_{j=1}^M f_j \right) * \left(\sum_{i=1}^{nME} P_{ME(i)} * C_{FME(i)} * SFC_{ME(i)} \right) + \left(P_{AE} * C_{FAE} * SFC_{AE} \right) + \left(\left(\prod_{j=1}^M f_j * \sum_{i=1}^{nPTI} P_{PTI(i)} - \sum_{i=1}^{nAE} P_{AEeff(i)} \right) * C_{FAE} * SFC_{AE} \right) \right] \cdot \left(\sum_{i=1}^{nAE} f_{eff(i)} * P_{eff(i)} * C_{FME} * SFC_{ME} \right) \cdot f_i * f_c * Capacity * V_{ref} * f_w$$

Table 1: Explanation of various terms of EEDI equation [20]

Main engine emissions	Auxilliary engine emission	Transport work
Shaft generators/ Motors emissions and energy saving technologies(Auxilliary power)		
Energy saving technologies(main power)		

Engine power(P)		Specific fuel consumption (SFC)
Individual engine power at 75% MCR		Fuel /unit of engine power (certified by manufacturer)
$P_{eff(i)}$	Main engine power reduction due to individual technologies mechanical energy efficiency	SFC_{ME} Main engine (composite)
$P_{AEeff(i)}$	Auxilliary engine power reduction due to individual technologies for electrical energy efficiency	SFC_{AE} Auxilliary engine
$P_{PTI(i)}$	Power of individual shaft motors divided by the efficiency of shaft generators	SFC_{AE*} Auxilliary engine (adjusted for shaft generators)
P_{AE}	Combined installed power of auxilliary engines	$SFC_{ME(i)}$ Main engine (individual)
$P_{ME(i)}$	Individual power of main engines	

Engine power(P)		CO_2 Emissions (C)
Individual engine power at 75% MCR		CO_2 emission factor based on type of fuel used by the given engine
$P_{eff(i)}$	Main engine power reduction due to individual technologies mechanical energy efficiency	C_{FME} Main engine composite fuel facto
$P_{AEeff(i)}$	Auxilliary engine power reduction due to individual technologies for electrical energy efficiency	C_{FAE} Auxilliary engine fuel factor.
$P_{PTI(i)}$	Power of individual shaft motors divided by the efficiency of shaft generators	$C_{FME(i)}$ Main engine individual fuel factors
P_{AE}	Combined installed power of auxilliary engines	
$P_{ME(i)}$	Individual power of main engines	

Correction and Adjustment factors (f)		Ship design parameters
Non dimensional factors that were added to the EEDI equation to account for specific existing or anticipated conditions that would otherwise skew individual ship's rating		
$f_{eff(i)}$	Availability factor of individual energy efficiency technologies (1 if readily available)	V_{ref} speed at maximum design load.
f_j	Correction factor for ship specific design elements. E.g: ice class ships require extra weight for thick hulls)	Capacity Dead weight tonnage (DWT) rating for bulk ships and tankers a percentage of DWT for container ship
f_w	Coefficient indicating the decrease in ship speed due to weather and environmental conditions.	
f_i	Capacity adjustment factor for any technical / regulatory limitation on capacity(=1 if none)	

* Detailed description can be found in IMO MEPC resolution 212(63), Annex 8.

2.3.3 Application and method of calculation

The attained EEDI shall be calculated for ships which falls into one or more of the categories of the vessels s mentioned in table 3 of 400GRT and above for,

- A ship for which the building contract is placed on 1January 2013 or,
- In the absence of a building contract the keel laid on or after 1 July 2013.
- The delivery of which is on or after 1 July 2015.
- substantially alters the dimension, carrying capacity or engine power or major repair.

EEDI value of new ships is required to be less than the baselines representing existing ships by a certain factor. Attained EEDI $\leq [(1-X/100) \times \text{Reference line value}]$ where X is the reduction factor as in table 3 and reference value in table 4. Values for bulk carrier is found in table 3 and similar reduction factors for others types of vessels are found in the Resolution MEPC 203 (62) of IMO.

Table 2: EEDI reduction factor in % (Bulk carrier) relative to Reference line, MEPC 203 (62).

Ship type	Size	Phase 0	Phase 1	Phase 2	Phase 3
		1Jan'13- 31 Dec'14	1Jan'15- 31 Dec'19	1Jan'20- 31 Dec'24	1Jan'25 onwards
Bulk carrier	≥ 20000 DWT	0	10	20	30
	10000-20000DWT	n/a	0 – 10*	0 – 20*	0 – 30*

* reduction factor to be linearly interpolated between the two values dependent upon vessel size. The lower value of the reduction factor is to be applied to the smaller ship size.

Table 3: Reference line value = axb^c , values of a, b, c MEPC 203 (62):

Ship type	A	b	c
Bulk carrier	961.79	DWT	0.477
Gas tanker	1120.0	DWT	0.456
Tanker	1218.8	DWT	0.488
Container ship	174.22	DWT	0.201
General cargo ship	107.48	DWT	0.216
Refrigerated cargo carrier	227.01	DWT	0.244
Combination carrier	1219.0	DWT	0.488
Ro-Ro cargo ships	1405.15	DWT	0.498
Ro-Ro Passenger ships	752.16	DWT	0.381
LNG carriers	2253.7	DWT	0.474
Vehicle / car carriers	(DWT/GT)- 0.7x780.36 where DWT/GT < 0.3 1812.63 where DWT/GT \geq 0.3	DWT	0.471
Cruise passenger having non conventional propulsion	170.84	GT	0.214

2.3.4 Reduction factors and implementation

At the beginning of phase I and at the midpoint of phase 2, IMO will review the status of technological development and if required amendments can be made to the time periods, the EEDI reference line parameters for relevant ship types and reduction rates set out in this regulation. Reduction factors will be used to implement the EEDI in phases so as to gradually reduce the required EEDI in much the same way as NO_x and SO_x limits. These reduction will apply to specific ship types and sizes as explained above. The fig shows the method of implementation over time.

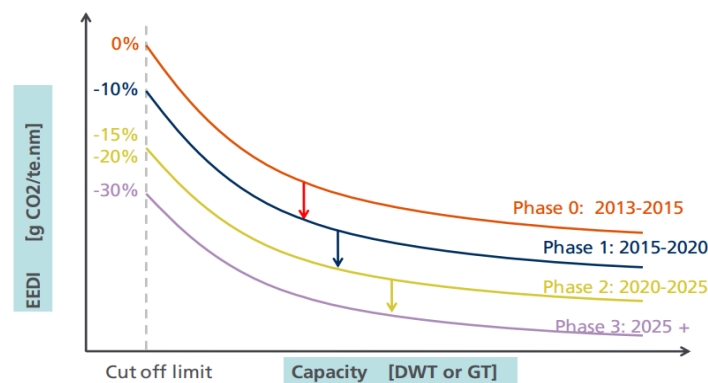


Figure 5: Reduction in phases (31)

2.3.5 Benefits

According to IMO the adoption of mandatory reduction measures for all ships from 2013 and onwards will lead to significant emission reductions and cost savings. It predicted that by 2020 annual CO₂ reductions would lie between 100 and 200 million tonnes due to the introduction of EEDI for new ships and the SEEMP for all ships in operation and by 2030 reductions will increase to between 230-420 million tonnes annually which is app 10-17% below business as usual by 2020 and between 19-26% in 2030. The reduction measures will also results in a significant saving in fuel costs to shipping industry. The annual fuel cost estimate gives an average figure of US\$50 billion by 2030.

2.3.6 Emission control measures other than CO₂ (IMO,EU and Class)

IMO has selected certain areas where more stringent rules are applied for type of fuels and emission of ships.

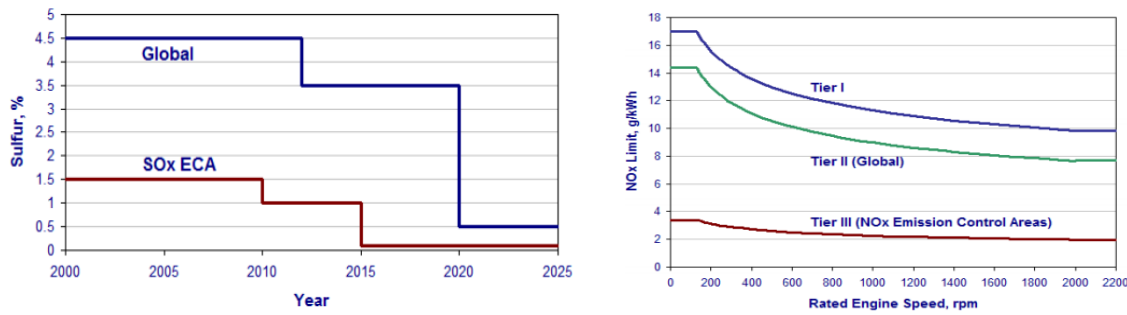


Figure 6: SOx and Nox emission limit in ECA

Thus two sets of emission and fuel requirements are defined by MARPOL Annex VI.1.Globally 2. In emission control areas (ECA), Baltic sea(SOx), North sea(SOx), North American ECA(NOx and SOx). NOx emission standards for diesel engines depends on engine maximum operating speed and are depends on engine RPM (n) as follows:

Table 4: NOx limit (Marpol- Annex VI)

Tier	Date	NOx limit g/kWh		
		N<130	130=n<2000	N=2000
Tier I	2000	17	$45 \times n^{-0.2}$	9.8
Tier II	2011	14.4	$44 \times n^{-0.23}$	7.7
Tier III	2016	3.4	$9 \times n^{-0.2}$	1.96

SOx emission standards is included in the MARPOL Annex VI regulations include caps on sulphur content of fuel as a measure to control SOx emissions . The sulphur limits on the fuel used and implementation dates are set as follows:

2.3.6.1 European Union activities and regulations by Classification societies

European Maritime Safety Agency (EMSA) monitors environment protection and pollution (30). It has set a target to reduce CO2 emissions by 20% by 2020 and has a strategy to reduce emissions from seagoing ships to reduce the emissions in the form of SO₂ (sulphur di oxide), NOx (Nitrous oxide) and particulate matter(PM). Their limits are more stringent to that proposed in MARPOL Annex VI.

ABS Enviro and Enviro+ notation comply with requirements of Annex I,II,IV,V,VI to the international convention for the prevention of pollution from ships. Class NK regulations regulations are more stringent than MARPOL NOx and SOx limits. Llyods register rules, Class notation by DNV additional class notations like CLEAN and CLEAN DESIGN which are voluntary and limits are stringent than specified by IMO.RINA's Green star and Green

Plus notation based on environment performance index procedures, to achieve an improvement in environmental performance beyond the level imposed by the IMO.

2.3.6.2 *Other standards*

The standards ISO 14001:2004 and ISO 14004:2004 deal with environmental management systems. The INTERTANKO CO₂ emission index, Clean ship index (clean ship project, Sweden), deals with SO_x, NO_x, Particulate matters, CO₂ emissions etc. Right ship environmental rating Similar to EEDI.

2.4 Energy efficiency methods

Optimum EEDI value can be achieved by reducing main, auxiliary engine and generator emissions, implementing efficient technologies, and optimizing transport work. This can be categorized into (i) Optimization approach, (ii) Energy saving devices (iii) Structural optimization and light weight construction (iv) Machinery technology (v) Fuel efficiency of ships in service.

2.4.1 Optimization approach

Table 5: Optimization approach

Optimizing ship particulars	Minimizing Hull resistance and increasing propulsion efficiency	Added resistance (waves & winds)
Ship size- Capacity Service speed	Optimizing the hull form, appendage resistance.	Assessing with waves.
Principal dimensions	Maneuvering considerations	Assessing with wind.

2.4.1.1 *Optimizing ship particulars and hull form*

Improvements in the computational tools enabled the user to optimize and explore alternative solutions taking in to consideration mainly hydrodynamics, by means of multi objective software. Economic studies, parametric series of design and life cycle cost assessments are applied in the design optimization. Fore body optimization includes bulb design, waterline entrance, forward shoulder and to the turn of bilge. Properly designed bulbous bow is very effective for reducing wave making resistance. Aft body optimization is done to mitigate sternwaves, improve flow into the propeller and avoid eddy effects. Potential solvers are used to evaluate wave making effects through aft shoulders however viscous calculations are needed to evaluate aftbody flow dominated viscous effects.

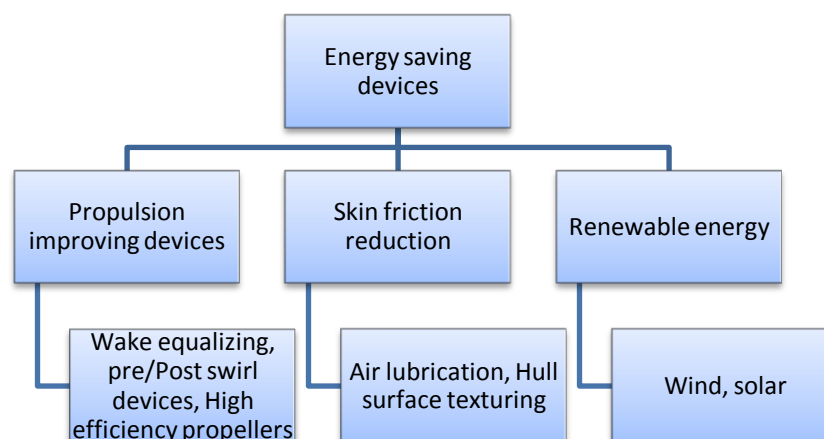
2.4.1.2 Ship size- Capacity and Service speed

If the ship's carrying capacity is increased with same service speed and cargo payload significant reductions of fuel consumptions per cargo volume can be achieved if larger ships are effectively utilized. For estimated cargo quantities per annum and a target fuel cost, the optimum design speed can be determined from an economic analysis called required freight rate analysis (RFR). This includes the ship construction, fuel, operating costs, port fees etc to meet the cargo demands at some speed, capital costs and operating costs.

2.4.1.3 Principal dimensions

Increasing the length/beam ratio and or increasing the length and reducing the block coefficient can provide reductions in propulsion fuel consumption as analyzed by [S.M.Rashidul Hasan](#) in his master thesis. A higher length/ beam ratio tends to reduce the wave making resistance while the reduced beam/draft ratio reduce the wetted surface area.

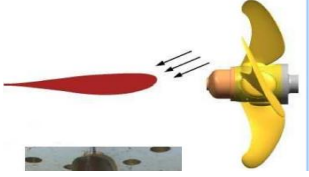






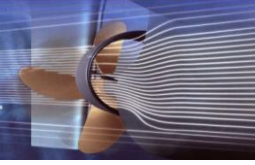
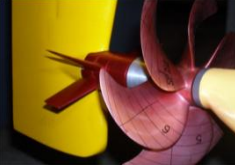
2.4.2 Energy saving devices



2.4.3 Propulsion improvement / Retrofit solutions working principle

The propulsive efficiency of ship is characterized by the Quasi propulsive coefficient (QPC) which is a function of open water hull and relative rotative efficiencies. Out of all these open water efficiency provides the greatest opportunity for improvement (17) because the other two parameters are generally close to 1 (around 0.9) . The open water efficiency is the product of ideal efficiency (based on axial momentum theory), losses due to fluid rotation induced by the propulsor and due to blade friction. Energy saving devices utilizes this principle by improving the efficiency by means of increasing the speed of flow or changing the direction of flow towards the propeller.

Table 6: Energy saving devices (17)

Twisted rudder	Rudder with costa bulb	Efficiency rudder
		
<p>-Regains the rotational energy in the propeller slip stream.</p> <p>-Reduces the drag of the rudder eliminating rudder cavitations.</p>	<p>- Reduce the hub vortex and reduce contraction of the propeller slipstream</p> <p>- Homogeneous axial slipstream and increased wake fraction.</p>	<p>- Reduce propeller inflow velocity. Hub drag is reduced by avoiding flow separation.</p> <p>- A more uniform and less contracted slipstream behind the propeller reduces losses in kinetic energy</p>
		
<p>Propeller Boss Cap Fin (PBCF)</p> <p>- Eliminates hub vortex</p> <p>-Recovers the kinetic energy of rotation of rotation flow around the boss.</p>	<p>Thrust fin</p> <p>- Recovers the kinetic energy due to the rotational flow</p> <p>-Deflects the flow from the propeller to turn its rotational components into useful axial flow</p>	<p>KAPPEL propellers</p> <p>-This has modified blade tip geometries aimed at suppressing the tip vortex and improving the overall propeller efficiency.</p>
<p>MHI Pre-swirl stator</p> 	<p>Wake equalizing duct (WED)</p> 	<p>Post swirl devices</p> 
<p>-Induce a tangential velocity in to the flow around the propeller plane.</p> <p>-This additional flow component acts to cancel out the tangential flow induced by the propeller maximizing the axial flow in the wake.</p>	<p>-The flow upstream of the propeller is characterized by areas of flow separations which gets finer towards the rear and the thrust deduction of the hull in general. WED placed in this region accelerates the water flow by directing it towards the area of maximum non uniformity of wake and make it homogeneous.</p>	<p>-Converts rotational components of flow created by the propeller to axial flow thereby reducing detrimental hub vortex and improve rudder efficiency.</p> <p>-In turn this reduces resistance from the rudder due to tangential flow from the propeller.</p>

2.4.4 Compatibility study

The devices presented are not always compatibility for specific ship designs are verified by model tests or CFD analysis to find correct functioning and understanding of the way they will interact with a design. Some devices remove the flow regimes upon which other work.

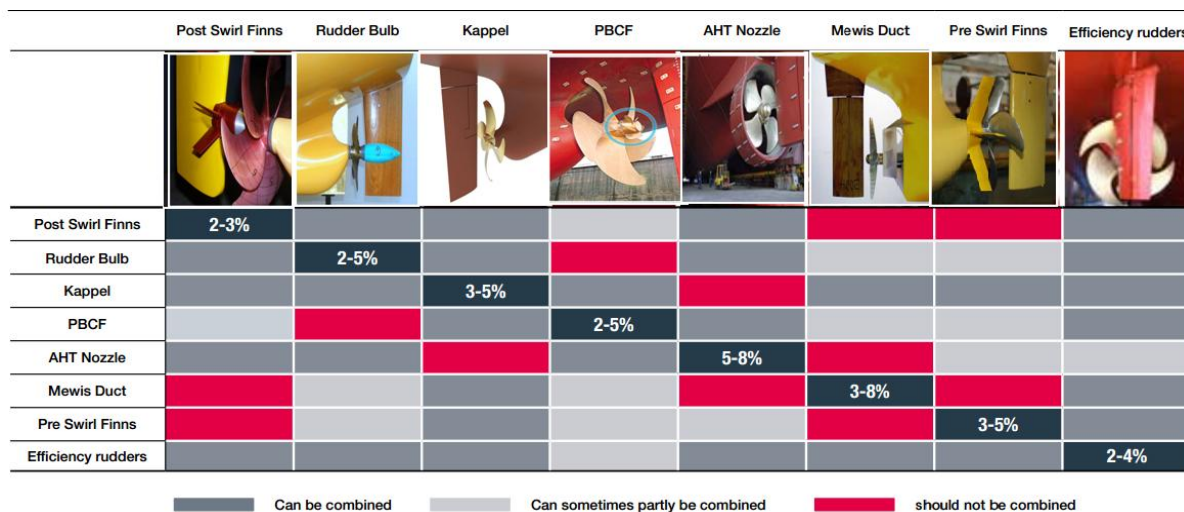


Figure 7: Compatibility study of energy saving devices ([MAN B&W presentation](#))

2.4.4.1 Skin friction reduction

Skin resistance depending on wetted surface accounts for the majority of total resistance, is significant for slower ships where the wave making resistance is small compared to the total and increases with the square of the speed. Reduced wetted surface, speed or the fluid interaction are effective. Paints reduce marine growth and improves the surface roughness (44).

Air cavity system and micro-bubbles A thin layer of air is maintained over the flat portion of the ship's bottom when a stable layer can be maintained significant reduction of skin friction and added resistance can be achieved at lower Froude number. micro bubbles reduces the density and improving viscous behavior of the water in contact with the hull by mixing it with air in the form of micro bubbles. (Drawback inability to maintain it for long distance).

Hull surface texturing: Flow velocity growth in the boundary layer is altered by adopting a surface texturing (riblets, micro cavities) in place of smooth hull and reduces the skin friction.

2.4.4.2 Renewable energy

Extra power is produced to propel the ship by flying a kite attached to the vessel's bow but launching, recovery and control are complex. Flettner rotors are vertical, cylindrical sails

spinning around their axis. A propulsive force is generated in the direction perpendicular to that of the wind hitting the rotor as a result of the magnus effect. PV panels gives low electric output per unit surface and are better suited as an additional source power.

2.4.5 Structural optimization and light weight construction

Structural weight reductions have a great effect on required power for both smaller vessels and displacement hulls. Use of higher strength steel, composites and nonferrous materials can reduce steel weight by 1.5-2 %, however the stress levels has to be addressed. FRP laminates and composites offer 30- 70% weight savings but recycling is the concerns.

2.4.6 Machinery technology Waste heat recovery

IMO regulations for NO_x , SO_x and CO₂ emissions was discussed earlier. Alternate solutions of LNG are of high initial investment. About 50% of the energy generated by the combustion of fuel oil being converted into mechanical energy and about 5% goes to exhaust gas. Improvements in turbo charger technology have also increased the heat available in the exhaust stream since they require less energy for the same boost than the older ones. A typical system is of exhaust gas boiler, steam or exhaust gas turbine ([Livanos et al](#)).

Table 7: EEDI and SEEMP related methods

	EEDI Reduction methods	SEEMP Related methods
1	Optimised hull dimensions and form	Engine tuning and monitoring
2	Light weight construction, design speed reduction	Hull condition
3	Hull coating, air lubrication system	Propeller condition
4	Optimization of propeller/ hull interface and flow device	Reduced auxilliary power
5	Contra rotating propeller	Speed reduction (operation)
6	Energy efficiency improvement	Trim/ draft
7	Waste heat recovery and Gas fuel (LNG)	Voyage execution
8	Solar, Wind power (sail, wind energy)	Weather routing
9	Hybrid electric power and propulsion concepts	Advanced hull coating
10	Reducing onboard power demand	Propeller upgrade and aft body flow devices

2.4.7 Success stories

Hull modification and subsequent numerical analyses performed for 19 versions of B573 ship was analyzed by Tadeusz et.al,(16) by modifying the hull form in stern part, block coefficient C_B , hull prismatic coefficient C_p and location of the longitudinal centre of buoyancy LCB with new body lines for each hull models resulted in a 2% decrease in hull resistance and 5% increase of screw propeller efficiency with a 8% reduction of EEDI value.

Mattia Brenner et.al (7) performed hydrodynamic optimisation of the ship's hull form by an optimization tool coupled with a potential CFD code for a high speed catamaran. The automated hydrodynamic optimization modified the shape of the ship's hull in an integrated CAD-CFD platform. The optimization code friendship frame work has a selection of variation (DoE) based on single and multi objective algorithm which selects the appropriate model by design constraints as input. The selected models are automatically tested with external CFD codes and the results are evaluated with the inbuilt post processor tool. They tested with a range of longitudinal and transverse side hull variables. This resulted in a improved wave pattern and a resistance reduction of 10% for the speed considered.

The author along with his colleague optimized a bulbous bow for a fishing vessel in an optimization code Mode-Frontier coupled with a potential solver REVA which evaluates ship resistance developed by Ecole Centrale de Nantes. By applying suitable constraints and an appropriate hyperbolic equation the designed bulbous bow reduced wave resistance by 5%.

MARIN (17) experimented with kites and concluded that large fuel saving is possible for slower ships like bulk carrier. Solar cells were tested on commercial vessel Auriga Leader, a car carrier of NYK Lines. The energy generated by the 40KW solar array is used to power lighting and other applications in living space. Maersk has recently devoted significant efforts to explore the viability of the micro bubble type of lubrication. MAN B&W (43) achieved great success in implementing kappel propellers for along with its engine and achieved greater fuel savings.

[Collison et al, 2013](#) tested Mewis and wake equalizing ducts with CFD and they claim an propulsive efficiency of 1.42%.

Various energy efficiency milestones has been achieved through European union projects Efforts, Fastpod, Streamline, Optipod, Targets, Grip over these years,

3 MODELING FLUID FLOW

The equations of fluid flow is a representation of three distinct non linear PDEs . Many assumptions and simplifications has to be made to obtain an incompressible fluid. Even in their reduced form the incompressible fluids case is still not trivial to solve. Along with the continuity equation the three equations create a complete mathematical system of governing in compressible flow. Because of the complexity of the Navier-Stokes equations including nonlinearity they are not easily solved analytically exception of few cases and a computational model is implemented for a numerical solution. In a non reduced form they form the complete mathematical model of flow.

3.1 Incompressible Navier -Stokes Equations

For in compressible flow the Navier-Stokes's equation are:

$$\rho \left[\frac{\partial u}{\partial t} + u \frac{\partial u}{\partial x} + v \frac{\partial u}{\partial y} + w \frac{\partial u}{\partial z} \right] = \rho f_x - \frac{\partial p}{\partial x} + \mu \left[\frac{\partial^2 u}{\partial x^2} + \frac{\partial^2 u}{\partial y^2} + \frac{\partial^2 u}{\partial z^2} \right]$$

$$\rho \left[\frac{\partial v}{\partial t} + u \frac{\partial v}{\partial x} + v \frac{\partial v}{\partial y} + w \frac{\partial v}{\partial z} \right] = \rho f_y - \frac{\partial p}{\partial y} + \mu \left[\frac{\partial^2 v}{\partial x^2} + \frac{\partial^2 v}{\partial y^2} + \frac{\partial^2 v}{\partial z^2} \right]$$

$$\rho \left[\frac{\partial w}{\partial t} + u \frac{\partial w}{\partial x} + v \frac{\partial w}{\partial y} + w \frac{\partial w}{\partial z} \right] = \rho f_z - \frac{\partial p}{\partial z} + \mu \left[\frac{\partial^2 w}{\partial x^2} + \frac{\partial^2 w}{\partial y^2} + \frac{\partial^2 w}{\partial z^2} \right]$$

With x_i ($i= 1,2,3$) in cartesian coordinates corresponding to (x,y,z) . u_i is the component of velocity, t is the time, p is the pressure, μ - Kineatic viscosity, ρ -density it can be expressed in indicial notation as:

$$\frac{\partial u_i}{\partial t} + u_i \frac{\partial u_i}{\partial x_i} = \frac{1}{\rho} \left(- \frac{\partial p}{\partial x_i} + \mu \frac{\partial^2 u_i}{\partial x_j^2} \right) + G \quad (1)$$

Two terms in LHS of the equation are a transient acceleration and a convective acceleration and a convective acceleration respectively. The first two terms on the RHS are pressure gradient and viscous term respectively. G represents the body force acting on the fluid.

The other equation needed to get a closed set of equations is the continuity equation and for incompressible fluid it is:

$$\frac{\partial u_i}{\partial x_i} = 0 \quad (2)$$

3.2 Reynolds averaged equations

Turbulent flow is agitated and disordered. Visually it is seen as eddies or vortices in the

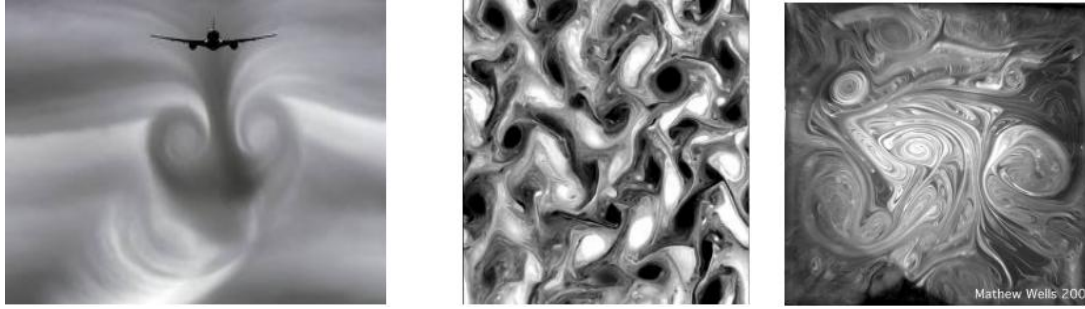


Figure 8: Vortex behind aircraft, turbulence on the Sun and chemical reactions

flow field and exists in scales of molecular to atmospheric motions. It is inherently time dependent [40] and in applications we are satisfied with the averaged flow in ensemble average as,

$$U_i = \bar{u}_i = \lim_{n \rightarrow \infty} \frac{1}{N} \sum_{n=1}^N u_i^{(n)}$$

Equation of the mean flow U_i can be started with dividing the flow into an average and fluctuating component u_i' as

$$u_i = \bar{u}_i + u_i' \text{ and } p = \bar{p} + p' \quad (3)$$

After introducing equation 3 in the Navier-Stokes equation 1 and further averaging results in

$$\begin{cases} \frac{\delta U_i}{\delta t} + U_j \frac{\delta U_i}{\delta x_j} = -\frac{1}{\rho} \frac{\delta P}{\delta x_i} + \frac{\delta}{\delta x_j} (\tau_{ij} - \overline{u_i u_j}) \\ \frac{\delta U_i}{\delta x_i} = 0 \end{cases} \quad (4)$$

where $\overline{u_i u_j}$ is the Reynolds stress. Thus the effect of the turbulence on the mean is through an additional stress R_{ij} written as:

$$[R_{ij}] = [\overline{u_i u_j}] = \begin{bmatrix} \bar{u}^2 & \overline{uv} & \overline{uw} \\ \overline{uv} & \bar{v}^2 & \overline{vw} \\ \overline{uw} & \overline{vw} & \bar{w}^2 \end{bmatrix} \quad (5)$$

The diagonal component in equation 5 is the kinetic energy of the turbulent fluctuations.

$$\bar{k} = \frac{R_{ii}}{2} = \frac{\overline{u_i u_i}}{2} = \frac{1}{2} (\bar{u}^2 + \bar{v}^2 + \bar{w}^2) \quad (6)$$

3.3 Turbulence modeling

Reynolds stress tensor will result in more unknowns called as a closure problem. Numerical methods are employed and the effects of the turbulence can be modeled since we are only interested in the mean. The simplest model is to introduce a turbulent viscosity as a proportionality constant between the Reynolds stress components and the strain rate tensor, in analogy with Newtonian fluids. Introducing this in to the Reynolds average equations gives

$$\frac{\delta U_i}{\delta t} + U_j \frac{\delta U_i}{\delta x_j} = \frac{\delta}{\delta x_j} \left[- \left(\frac{P}{\rho} + \frac{2}{3} k \right) \delta_{ij} + (v + v_T) \overline{E_{ij}} \right] = - \frac{1}{\rho} \frac{\delta P}{\delta x_i} + (v + v_T) \nabla^2 U_i \quad (7)$$

$\overline{E_{ij}}$ in equation 7 is the deformation tensor calculated based on the mean flow. The turbulent viscosity v_T must be modeled and most numerical codes which solves for the Navier-Stokes equations for practical applications uses some kind of model for v_T . For simple shear flows velocity fields of the form $U(y)$ the main Reynolds stress component becomes

$$\overline{u'v'} = -v_T \frac{\delta U}{\delta y}, \text{ in analogy with kinetic gas theory, } v_T = u_T l$$

where u_T is a characteristic turbulent viscosity scale and l is a characteristic turbulent length scale. In kinetic gas theory l would be the mean free path of the molecules and u_T the characteristic velocity of the molecules.

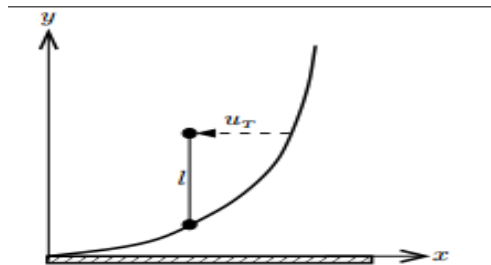


Figure 9: Prandtl's mixing length l (40)

3.3.1 Zero equation models

The simplest models for u_T and l is to be model them algebraically. In simple free shear flows v_T taken as constant in normal direction or y direction and to vary in a similar manner in x . In wall bounded shear flow we can take l as Prandtl's mixing length, a distance over which the over which the particle retains its momentum and is depicted in the above figure 9.

(40) Prandtl mixing length is the length where fluid displaced in the normal direction retains its horizontal momentum.

3.3.2 One equation models

Instead of modeling the characteristic turbulent velocity algebraically here it is assumed u_T a value and a differential equation is used to calculate ϵ , a mean dissipation rate of the turbulent kinetic energy. By this new unknowns would be introduced and are modeled as follows:

- First we model the Reynold's stress as in equation 7,

$$\overline{u_i u_j} = \frac{2}{3} \bar{k} \delta_{ij} - v_T \left(\frac{\delta u_i}{\delta x_j} + \frac{\delta u_j}{\delta x_i} \right)$$

- Second the turbulent dissipation is modeled based on dimension using \bar{k} and l.

$$\epsilon = C_D \frac{\bar{k}^{-3/2}}{l} \quad (\text{dimension of } \epsilon \text{ is } \epsilon = \frac{L^2}{T}, C_D \text{ is the modeling constant}).$$

- Third a gradient diffusion model is used for the transport terms i.e.

$$-\frac{1}{2} \overline{u_i \cdot u_i \cdot u_j} - \frac{1}{\rho} \overline{p u_j} = \frac{v_T}{Pr_k} \frac{\delta \bar{k}}{\delta x_j} \quad (Pr_k \text{ is the turbulent Prandtl number}).$$

In simple terms the resulting equation for the turbulent kinetic energy for constant v_T can be written as:

$$\frac{D\bar{k}}{Dt} = (v + v_T) \nabla^2 \bar{k} - \overline{u_i \cdot u_j} \frac{\delta u_i}{\delta x_j} - \epsilon \quad (8)$$

Rate of increase diffusion rate generation rate dissipation rate

3.3.3 Two equation models

The most popular model is two equation ($\bar{k} - \epsilon$) model which is based on the one equation model for \bar{k} but instead of modeling ϵ a partial differential equation is derived governing the turbulent dissipation. This equation has the form as the equation \bar{k} with a diffusion term a generation term and a dissipation term. Many new model constants need to be introduced in order to close the ϵ equation. Once \bar{k} and ϵ is calculated the turbulent viscosity is evaluated as a quotient of the two with C_μ the modeling constant as:

$$v_T = C_\mu \frac{\bar{k}^2}{\epsilon} \quad (9)$$

3.3.4 Reynold's stress models

It solves a system of 7 equations to calculate all Reynold's stress. Only 6 stress need to be solved for since the stress matrix is symmetric and a seventh equation is solved to determine

the specific dissipation. The model is known as a second order closure model. While the Reynold's stresses are modeled the model does not perform well for wall bounded flows.

3.4 Wall region

The Law of the Wall states that the average velocity of a turbulent flow is proportional to the distance from that point to the wall. In general the law of wall is only valid for the first 20% of the flow height from the wall. In most cases the law takes a general logarithmic formulation where the velocity at a distance from the wall is given as

$$u^+ = \frac{1}{k} \ln y^+ C^+ \quad (\text{where } y^+ = \frac{yu_r}{\nu}, \quad u_r = \sqrt{\frac{\tau_w}{\rho}}, \quad u^+ = \frac{u}{u_r}).$$

Further in implementation the model is modified to account for the velocity in the viscous sublayer, $y^+ \leq 5$. In this region u^+ is taken as y^+ .

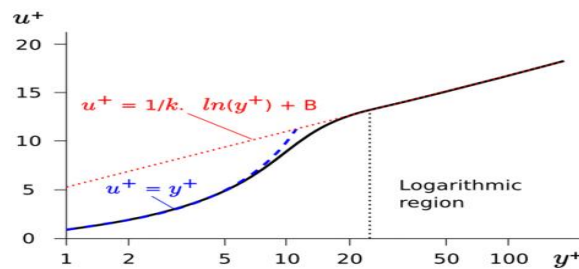


Figure 10: Velocity profile in logarithmic region[36]

Other mean flow quantities such a temperature and production of turbulent kinetic energy can then predicted based on this assumed velocity profile. It should be noted that when the law of the model used in the solution these assumed profiles and their associated quantities will influence the calculated wall values. Depending on the near wall mesh resolution in practice there are typically three methods used for implementation of the law of the wall [36]:

High y^+ model assumes that the centroid of the near wall cell lies in the logarithmic region $y^+ > 30$.

Low y^+ model assumes that the mesh is resolved to the viscous sublayer. In this case wall laws are not used. While theoretically this occurs at $y^+ < 5$, in practice the mesh normal to the wall should be resolved enough to produce solution y^+ values less than 1.

All y^+ model attempts to mimic the behaviour of both the high and low y^+ models to allow for relatively coarse grids with flows that have a reduced friction velocity. Most of them

contain a functional blending treatment to better represent the velocity between the viscous sublayer and the logarithmic regions.

3.5 Brief introduction of various solution methods in Star-CCM+

3.5.1 Finite Volume Method

Finite method utilizes the integral form of the conservation laws (Navier-Stokes equations) by separating a computational domain into a series of finite arbitrary control volumes without change of the coordinate system. The basic methodology can be explained as continuity equation of an incompressible flow can be converted into an integral form over a control volume and applying the divergence theorem we obtain $\oint_{S_i} v \cdot \eta ds = 0$ (η is a unit normal) and the finite volume approximations of this surface integral would be required on a cell by cell basis by using suitable quadrature formula and result a system of algebraic equations. The method used in Star-CCM+ is of second order accurate in space depending on the convection differencing scheme used. Whenever possible the second order linear CDS is used but sometimes order of accuracy had to be decreased to stabilize the simulation. The time stepping algorithm is second order accurate in time and is implicit.

3.5.2 Velocity pressure coupling & basic principle of SIMPLE algorithm:

Discretised form of the Navier-Stokes equation the form of equations show linear dependence of velocity on pressure and vice versa [15]. This inter equation is called velocity pressure coupling. SIMPLE is one of the solution methods for this problem. Discretization of Navier-Stokes equations for incompressible flow equation reduces to equations containing velocity and pressure coupled and it is solved as,

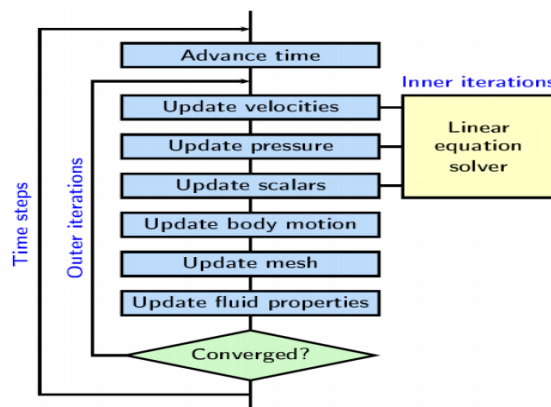


Figure 11: Iterative solution method for a coupled simulation of flow. (Morch et al. 2008)

- In the predictor step the pressure field at t^{n-1} is used to solve the momentum equation, resulting in an intermediate velocity field. This velocity field will in general not satisfy the continuity equation.
- In the first corrector step a pressure correction equation is solved to obtain a correction for the pressure field. The pressure field is updated using this correction and using under-relaxation.
- This velocity field is updated using the correction for the pressure field.

The iterative process is repeated until the change in the variable from one iteration to the next becomes small that the solution can be considered converged. At this point all discrete conservation equations are obeyed in all cells to a specified tolerance and doesn't change.

3.5.3 Mesh generation

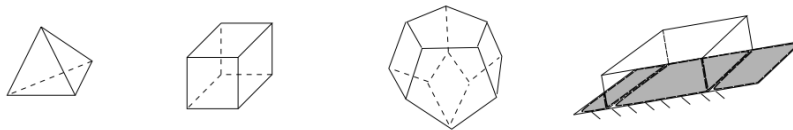


Figure 12: Different cell types, From left to right: Tetrahedral, hexahedral, polyhedral and prism. [27]

For making a mesh a volume mesh generator as well as surface treatment tools are used. In order to make a grid a 3D surface file can be imported which is the geometry to be modeled. The surface mesher then utilizes the surface to make a refined mesh and this mesh forms the starting point for generation of the volume mesh. The mesh used in this thesis are:

3.5.3.1 Trimmed mesher

Trimmer meshing technique [27] makes use of a template mesh constructed from hexahedral cells. From that template the mesher trims the required core mesh utilizing the starting geometry as reference. The resulting mesh is composed of hexahedral cells with trimmed cells close to the surface. These cells are generally polyhedral cells with one or more edges cut off. It provides a robust and efficient method of producing a high quality grid for both simple and complex mesh generation problems eg: cell refinement in the wake region around propeller.

3.5.3.2 Polyhedral

Polyhedral topologies are developed by combining multiple tetrahedral to form a polyhedral volume [28]. It is automatically created from an underlying tetrahedral surface mesh. Form a

solution standpoint it offers better results than tetrahedral. For a number of cases this is the default mesh topology due to the solution advantages and the ability to create conformal interfaces using automeshers.

3.5.3.3 Prism layer

This mesher makes one or more layers of fine orthogonal prismatic layers next to the wall boundaries. Generally a subsurface is generated at the user specified prism layer thickness before the core volume mesh is developed. Using this subsurface the core mesh is constructed by any of the chosen volume meshers. As a next step the prism layer is generated by extruding the cell faces from the generated core mesh to the original starting surface. This mesh model produces higher aspect ratios close to the wall where boundary layer has a great influence and thereby improving the solution.

3.5.4 Volume of fluid method

The equation to be solved contains only rate of change and convective terms and its role is to track the deformation of the initially flat free surface [10]. The convective terms are discretized using the HRIC scheme (Muzafarjia and Peric,1999).

3.5.4.1 Free surface modelling

Star CCM+ uses [12] a two-phase Volume of Fluid (VOF) method to calculate the location of the water surface (resolve the boundary between two phases of liquid) as proposed by [Hirt and Nicholas 1981]. A free boundary can be an interface between two fluids like for free surface flow or it can be the interface between materials like for free-surface flow or it can be the interface between materials or between fluid and a deformable surface.

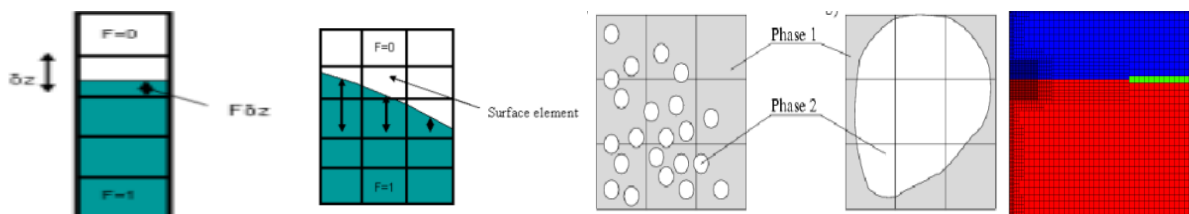


Figure 13: Grids unsuitable(L) and suitable (R) for 2phase flows in VOF model (CD-Adapco 2011)

For each cell in the grid a water fraction function F is defined so that F is 1 if the cell is filled with fluid and 0 otherwise. A cell partly filled with fluid has a water fraction between 1 and 0. It is thus clear that cells with a fraction other than 1 or 0 must contain a free water surface. The exact position of the surface can then be calculated. As illustrated in figure 13 this is

straight forward for one dimensional column. The location of the water surface location simply becomes the level of the bottom of the cell + F times the vertical size of the cell. for 2D and 3D case the calculation is bit more involved because the slope of the water in a cell is not given however the principle is the same.

For a transient simulation the fluid fraction of each cell can be calculated by the equation 10 in 2D (Hirt and Nicholas 1981).

$$\frac{\partial F}{\partial t} + u_1 \frac{\partial F}{\partial x_1} + u_2 \frac{\partial F}{\partial x_2} = 0 \quad (10)$$

3.5.4.2 Limitations

This method is suitable for simulations of flows where each phase constitutes a large structure with a relatively small contact area between phases as in figure 13. An assumption for the VOF method is that both phases share the same velocities, pressure and temperature within a control volume (Hirt and Nicholas [1981](#)). This assumption will lead to large errors if the fluid bodies are small compared to the fineness of the grid. At least three cells should be used across the water body to get good results and is the reason for finer mesh in the free surface.

3.5.4.3 Applicability for ship related motions

In most of the simulations presented later the ship or the propeller operates in the vicinity of the free surface. Hence the location of the free surface has to be determined during the simulation by VoF method. The interpolation of the face values from the cell centres is more complex than for other properties and requires a special interpolation scheme. The spatial distribution of each phase at a given time is defined in terms of a variable called the volume fraction as explained above. A method of calculating such distributions is to solve a transport equation for the phase volume fraction. For this the method used in Star-CCM+ is segregated flow model. This solves the flow equations in a segregated or coupled manner.

3.5.5 Simulating rotation

3.5.5.1 Moving Reference Frame

Moving reference frame (MRF) method involves rewriting the time averaged steady state form of the Navier-Stokes equations in a moving frame [\[28\]](#).

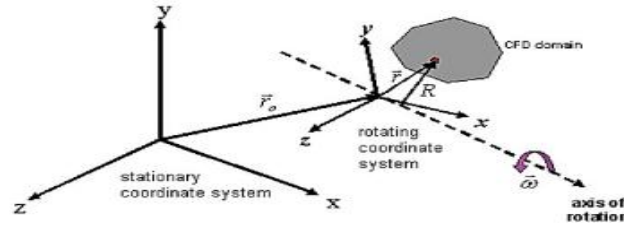


Figure 14: Rotating coordinate system in a moving reference frame [28]

For a rotating frame with constant rotational speed the equations are transformed into a rotating frame to get a steady state solution. It does not take into account any unsteady components of the flow field thereby serving as a preliminary solution to the unsteady problems. Its versatility and low CPU demand makes it in widespread use in the turbo machinery problem.

Consider a coordinate system rotating an angular velocity ω relative to the stationary reference frame as shown in the figure. The origin of the rotating system is located a position vector r_0 with r being the position of an arbitrary point from the origin of the rotating frame. To transform the equations of motion the fluid velocities are written in a rotating frame as

$$v_r = v - (\omega \times r) \quad (11)$$

where v_r is the relative velocity viewed from the rotating frame and v is the absolute velocity viewed from the stationary frame. Using the equation 11 the mass and momentum equations are rewritten as

$$\begin{aligned} \frac{\partial \rho}{\partial t} + \nabla \cdot \rho v_r &= 0 \\ \frac{\partial}{\partial t}(\rho v_r) + \nabla \cdot (\rho v_r v_r) + \rho(2\omega \times v_r + \omega \times \omega \times r) &= -\nabla p + \nabla \cdot \tau \end{aligned} \quad (12)$$

Two additional acceleration terms (coriolis and centripetal) are introduced to the momentum equation. The remaining components of the equations remain consistent with the stationary frame Navier-Stokes equations except with the introduction of the relative velocity.

3.5.5.2 Sliding Mesh

Sliding mesh (SLM) approach involves accurate time dependent simulations where the unsteady interactions of the fluid flow are considered [28]. This involves setting one grid domain inside the computational domain with a relative motion with respect to the adjacent

grid domain. For the code to be able to transport fluid variables between both grid domains, an interface is introduced to perform the interpolation.

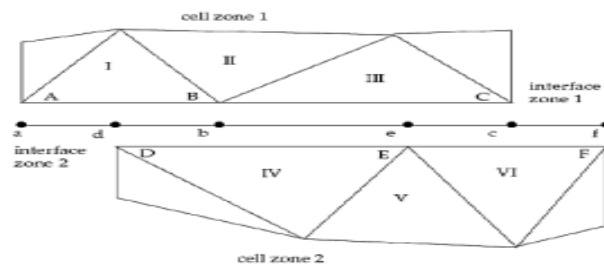


Figure 15: Sliding mesh between two domains with relative motions [28]

At every time step the unsteady RANS equations are solved in each cell zone and the fluxes are calculated across the faces over the interfaces. However at the next time step the grid domain with a relative motion will move to a new location and the grid points are no longer aligned. This will require the interface zone to perform interpolation in order to transfer the fluxes between the two grid domains. This happens at every time step and makes this approach computationally demanding.

3.5.6 Simulation of flow with rotating geometries

Flow problem of rotating propeller behind the ship because of the 3-D highly unsteady complex phenomena and the relative motion between the rotating geometry and the stationary configuration makes it difficult to compute with single fixed grid system. Earlier numerical techniques [11] for simulating this type of flow is modeled where the rotating propeller is excluded from the computational domain and its effect on the flow is modeled by either experimentally measured flow quantities or alternatively by empirically defined source terms distributed throughout its volume. Although these methods yielded reasonable results they are subjected to the serious drawbacks in the empiricism associated with these procedures. Advancements in computer technology now makes it feasible to solve complex mathematical formulation effectively there by nowadays propeller is modeled as it is without any simplification as done in [11].

3.5.7 Scaling laws

3.5.7.1 Geometric similarity

Geometric similarity assures that the model and full scale ship are geometrically similar by a scale factor constant between model and prototype. This requirement is also valid for the surrounding medium. Thus waves, water depth and hull roughness are modeled with the same scale factor. $\lambda = \frac{l_s}{l_m}$. In actual practice there are some difficulties to achieve this and corrections are made. Eg: Hull roughness correction ΔC_F .

3.5.7.2 Kinematic similarity

Kinematic similarity requires equal ratios between velocities in model and full scale. Flow around the hull will undergo similar motions in both model and full scale. Eg: advance coefficient J used in propeller model tests.

3.5.7.3 Dynamic similarity

Dynamic similarity requirement states that the ratio between the forces should be equal in both model and full scale for the flow to be similar. If we consider an example of ship resistance test different kind influencing forces are inertia, gravity and viscosity.

$$(i) \frac{Inertia}{gravity} = \frac{\rho U^2 l^2}{g l^3 \rho} = \frac{U^2}{g l} \quad (ii) \frac{Inertia}{Viscosity} = \frac{\rho U^2 l^2}{\mu U l} = \frac{\rho U l}{\mu} \quad (iii) \frac{Gravity}{Viscosity} = \left(\frac{Inertia}{gravity} \right)^{-1} \frac{Inertia}{Viscosity}$$

The third ratio is a combination of the first two. So if the first two ratios are respected the last one will also be. The first ratio is almost the Froude number and that the second number is the Reynolds number with μ the dynamic viscosity.

$$Fr_M = \frac{U_M}{\sqrt{g l_M}} = Fr_S = \frac{U_S}{\sqrt{g l_S}} \quad (\text{subscript M - model and S- ship, ratio of the length scale } \lambda = \frac{l_S}{l_M}).$$

$$\Rightarrow U_M = U_S \sqrt{\frac{g l_M}{g l_S}} = \frac{U_S}{\sqrt{\lambda}} \quad (\text{speed for the model can be determined by the speed of the real ship}).$$

To respect the Reynold's number we can take into account the relation as found before:

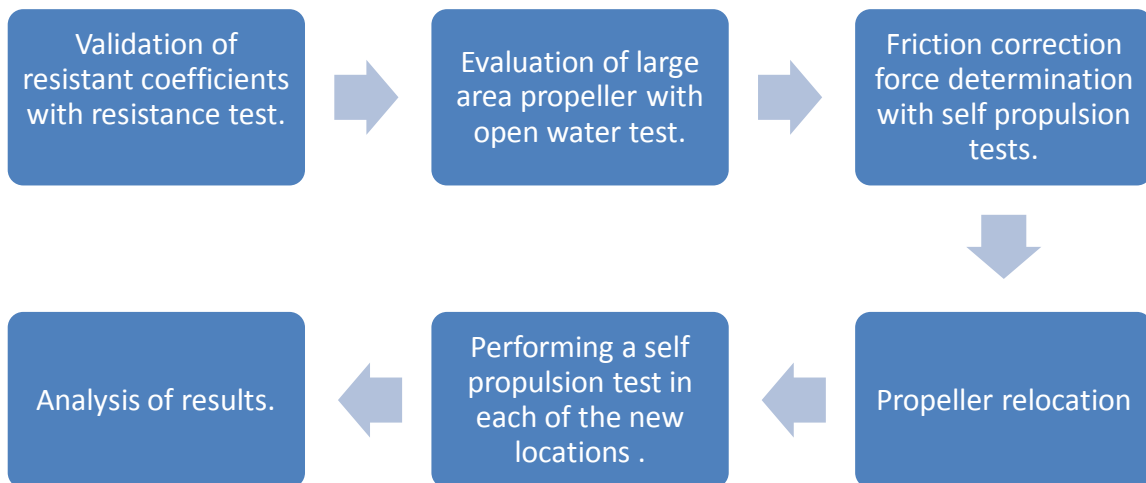
$$Re_M = \frac{U_M l_M}{\gamma_M} = Re_S = \frac{U_S l_S}{\gamma_S} \Rightarrow \gamma_M = \gamma_S \frac{U_M l_M}{U_S l_S} = \frac{\gamma_S}{\lambda^{\frac{3}{2}}}$$

So if we want to respect the Froude number, we should change the viscosity of the fluid to respect also the Reynolds number. It is not practically feasible. So in towing tank we respect Froude number and we artificially impose turbulence by some artificial means.

4 WORK FLOW ANALYSIS

The objective is to numerically simulate the self propulsion and the associated tests. The simulations were validated with experimental results at each stage. The resistance, open water and self propulsion tests were performed in a model scale and based on the results it was determined to perform in a full scale as a continuation of this work. Due to the time constraints involved it was not able to perform in this work.

The tests were carried out in a research vessel MS Nawigator belonging to University of Szczecin and the propeller was a indigenous design of Ship Design and Research Centre (CTO S.A). The 3D CAD file was developed in NAPA IGES format throughout the master thesis work and will not be referred explicitly hence forth.



4.1 Numerical setup:

Memory: 16GB DDR3- 1600 RAM.

Processor: Intel® Core i5-4570 CPU @3.2 GHZ (4 core).

Software used: Star-CCM+ (Version 9.04.009)

5 RESISTANCE TEST

It is performed to determine the ship resistance in model scale and extrapolate them into a full scale to predict the required power to propel the ship.

5.1 Setup and test procedure

The resistance test is performed on the basis of geometric, kinematic and dynamic similarity. Geometrical similar scaled model is towed at Froude scaled speeds to ensure correctly scaled wave resistance. The model is attached to a towing carriage by a dynamometer that measures the resistance during the test. Further the vessel speed is recorded and the two values are the input to the scaling procedure from the resistance test. These values will be used to determine the residuary resistance coefficient which is assumed equal in model and full scale to give an estimation of the required power for the ship.

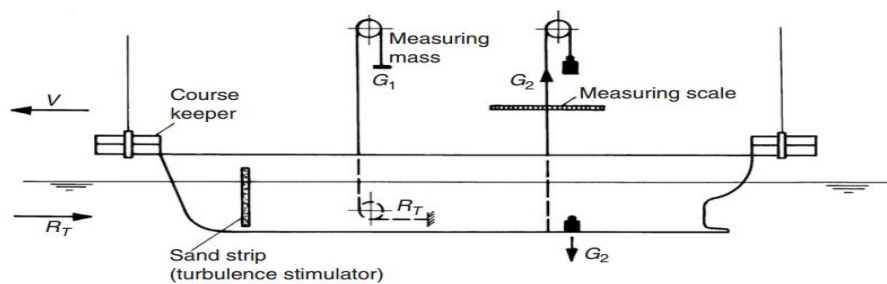


Figure 16: Resistance test experimental setup (47)

5.1.1 Expression of the resistance:

Viscous and residuary drags are independent. The former is due to the friction of the water on the hull and the later concerns the waves and factors other than friction. We commonly work with the resistance coefficient instead of resistance itself. The resistance coefficient is,

$$C_{Resistance} = \frac{Resistance}{\frac{1}{2}\rho V^2 S} \quad (13)$$

(resistance in Newton, ρ the density of the water kg/m^3 , V the speed and S the wetted area). The interest of the coefficient is that it is non dimensional so it is easy to compare. So Froude considered that the coefficient of total resistance is the sum of the coefficient of the residuary drag depending on the Froude number only and friction drag on the Reynolds number only:

$$C_T(Re, Fr) = C_F(Re) + C_R(Fr) \quad (14)$$

5.1.2 ITTC 57 method

5.1.2.1 Frictional drag

Friction depends on the wetted area. A vertical plate has been tested (no residuary resistance) and with a curve fitting approach friction drag coefficient is given by $C_F = \frac{0.075}{(\log^{10} Re - 2)^2}$

5.1.2.2 Method of calculation

Following the towing tank tests knowing the characteristics of the hull and the total resistance we can calculate the coefficient of total resistance for the model:

$$C_{TM} = \frac{R_{TM}}{\frac{1}{2} \rho_M V_M^2 \rho S_M} \quad (15)$$

With the frictional coefficient deducted as in section 6.1.2.1 for the model, we can obtain the coefficient of residuary resistance for the model equal to that of ship with Froude's similarity. Finally the resistance of real ship is calculated as,

$$C_{TS} = C_{RS} + C_{FS} + \Delta C_F$$

5.1.3 ITTC 78 method

The Froude assumption has been changed. Friction was divided into residuary and friction drags later calculated after tests [\(23\)](#). But when a flat plate pulled the increase of the boundary layer thickness creates form drag. Previously it was included in the residuary resistance (even if it depends on the Reynolds number). Here they preferred to consider it with friction. So the total friction coefficient is the function of the frictional resistance and wave drag.

$$C_T(Re, Fr) = (1 + k)C_{FO}(Re) + C_W(Fr) \quad (16)$$

5.1.3.1 Method of calculation:

1. The total resistance and the friction coefficient determined by ITTC-57 method.
2. Determine the form factor (k) by empirical, low speed test or Prohaska's methods.
3. Calculate the coefficient of wave resistance for the model equal by assumption to the one of the ship: $C_{WM} = C_{TM} - (1 + k)C_{FM} = C_S$
4. Calculate the coefficient of frictional resistance of the ship.

5. Resistance coefficient computed with roughness allowance and air resistance coefficients ΔC_F and C_{AA} as mentioned in the ITTC procedure as $C_{TS} = (1 + k)C_{FS} + C_{WS} + \Delta C_F + C_{AA}$ and the global resistance can be found.

5.2 Experiments

Resistance coefficient C_T obtained in this experiment is a key parameter of friction correction force [$F_D = 0.5 \rho_M v_M^2 S_M (C_{TM} - C_{TS})$] based on which self propulsion test is done. The presented results forms the base for validating numerical tests.

Table 8: Resistance test results determined at CTO S.A during a test performed earlier

Ship data (MS Navigator XXI)		Model and test data		
Length LWL (m)	55.16	Scale factor		10
Draught TF/TA (m)	3.15/3.2	Appendages		None
Displacement (m ³)	1126.3			
Wetted surface(m ²)	670.0	Water	Sea	Tank
Bilge keel area (m ²)	25.0	Temperature(Cel)	8	13.4
Area above WL (m ²)	130.0	Mass Density (kg/m ³)	1027.1	999.3
Form factor (Prohaskha's)	0.25	Kin. Visc ($\times 10^{-6}$) m ² /sec	1.43079	1.18859
Roughness allowance($\times 10^3$)	0.721	Air res co. eff($\times 10^{-3}$)		0.193

Values for model							
V_S (Knots)	V_M (m/sec)	R_{TM} (N)	$C_{TM}(\times 10^{-3})$	$RN_M(\times 10^6)$	$C_{FM}(\times 10^{-3})$	$C_R(\times 10^{-3})$	Fn
10	1.627	42.953	4.8347	7.5491	3.1521	1.3674	0.2212
11	1.789	55.505	5.1633	8.304	3.0993	1.7541	0.2433
12	1.952	70.411	5.5037	9.0589	3.0522	2.1463	0.2654
13	2.115	96.496	6.4269	9.8138	3.0098	3.1161	0.2875
Extrapolated for ship (values for the ship hull roughness 120×10^{-6} m)							
V_S (Knots)	RT_S (KN)	PE (KW)	$C_{TS}(\times 10^{-3})$	$RN(\times 10^8)$	$C_{FS}(\times 10^{-3})$		
10	42.91	220.8	4.6996	1.9831	1.8912		
11	55.89	316.2	5.0582	2.1814	1.866		
12	71.34	440.4	5.4252	2.3797	1.8446		
13	98.34	657.6	6.3723	2.5781	1.8246		

5.3 Resistance test Star- CCM+

It is performed to determine the total resistance coefficient (C_T), trim and heel in model scale of the research vessel M/S Nawigator XXI. In addition wake field at propeller plane and free surface flow around a ship is predicted in a initially calm water taking heave and pitch motion into consideration.

5.3.1 Creation of computational domain

The fluid domain extends $0.5L$ on top, L forward and bottom, $2L$ aft, port and star board where L is the length between perpendiculars resulted in $24\text{m} \times 12\text{m} \times 11\text{m}$ created around the model for a symmetry (12). Then the other symmetry of the ship is subtracted from the model thus one half of the domain is used for simulation and the surfaces of the fluid domain is divided into regions as outlet for the back of the ship symmetric surface on the symmetric plane, inlet surface forward, top, bottom and side.

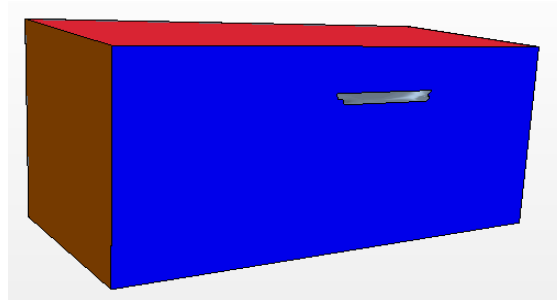


Figure 17: Fluid domain

5.3.2 Generating the volume mesh

Resistance analysis are generally performed using a trimmed volume mesh with prism layers on the wetted surface of the hull. By using trimmed cells the mesh is aligned with the undisturbed free surface. Tables 9 and 10 describes key mesh parameters.

Table 9: Mesh parameters (Surface remesher- Trimmer- Prism layer)

Base Size	0.3m
No Prism Layers	6
Prism Layer Thickness (% of base)	5
Minimum/ Target surface Size (% of base)	25/100

Table 10: Local mesh settings at boundary

Boundary	Prism mesh	Surface mesh	
		Relative min size (%)	Relative target size (%)
Deck	Default values	25	100
Hull, transom	Default values	8	100
Top, bottom, side, symmetric, inlet, outlet.	Disabled	25	1000

5.3.2.1 Volumetric controls for local refinement

In order to improve the resolution of flow features like flow separation or the Kelvin wave the volumetric refinements were applied to the mesh. The free surface area that is the interface between the water and air is also refined. By using trimmed cells we can take the advantage of anisotropic refinement in the normal of the free surface area. We have defined the geometrical shapes and dimensions of these volumetric controls in the form of part shapes. These shapes were created in the regions near bow, free surface, hull, wake waves for predicting those intended for. By this procedure the physics is captured accurately with optimum usage of number of elements in the mesh.

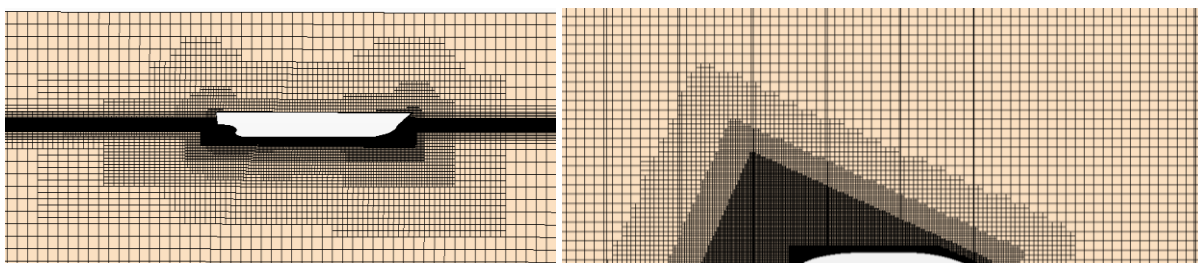


Figure 18: Volumetric refinement created for waves

Table 11: Volumetric mesh refinement

	Refinement levels	Trimmer	Relative Size(% base)
Bow	5	Isotropic	3.125-50
Free Surface	4	An-Isotropic	Z Size-(1.5625 to 12.5)
Hull	5	An-Isotropic	X Size- (6.25-100),Y,Z Size-(3.125-50)
Wake	1	Isotropic	Rel size- 3.125
Waves	3	An-Isotropic	X,Y Size-(12.5-50)

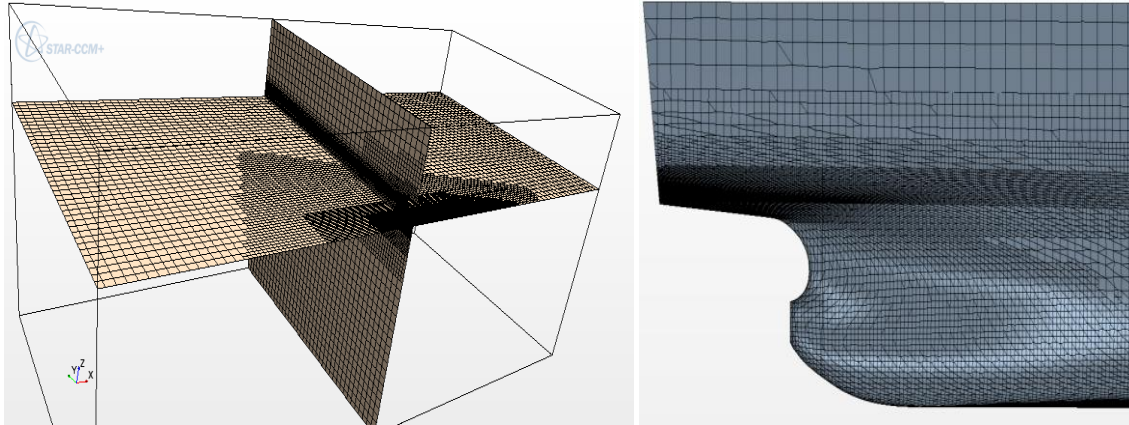


Figure 19: fig (L) section at water line fig (R) Surface mesh refinement at aft

Table 12: Boundary definition

Boundary	Boundary Type
Tank Inlet	Velocity Inlet
Tank Outlet	Pressure Outlet
Tank Side	Wall
Tank symmetry	Symmetry Plane
Tank Top	Wall

5.3.2.2 *Selecting the Physics Models*

The model is selected as Implicit unsteady, Eulerian Multi Phase, Volume Of Fluid, Turbulent, K-Epsilon Turbulence, Gravity, VOF waves.

5.3.2.3 *Defining the Eulerian Phases*

Using the VOF multi phase model Eulerian phases created for water and air.

5.3.2.4 *Defining VOF wave*

The free surface water level changes over time during the simulation. Using VOF model ([section 4.5.4](#)) wave initial and boundary conditions were specified. Here the ship is towed through calm water. Therefore a flat VOF wave is specified. Also the current and air is specified according to the velocity as decided before.

5.3.2.5 *Damping wave reflections*

The wave reflections must be avoided because they interact with the true wave field and give invalid results. Thus VOF wave damping at boundaries were specified in the region.

5.3.2.6 Defining Dynamic Fluid Body Interaction(DFBI)

This model simulates the motion of the ship according to the forces acting on it inducing the flow. For this the ship is allowed to move with two degrees of freedom to account for sinkage and trim. The initial conditions of the 6 DOF body are mentioned in table 13.

Table 13: DOF set up

Centre of mass	[2.66, 0.0, 0.05] m, m, m
Moment of Inertia	[950.0, 950.0, 950.0] kg/m ²
Body mass	561.78 kg
Release Time	2sec
Ramp time	0.5 Sec

A new coordinate system is created at the centre of mass as origin. The creation of the new 6DOF body automatically creates a body local coordinate system and is located at the centre of mass of the body and moves with the body as the simulation process. To define the free motion of the ship it is allowed to heave in Z direction and rotate along the Y axis.

5.3.2.7 Setting solver parameters and stopping criteria

The resistance prediction is a transient simulation for which the time step, the number of inner iterations per time step and the physical time is setup. Also the under relaxation factors are setup to enhance the convergence per time step as mentioned in table 14.

Table 14: Under relaxation factor

Time step, Number of inner iterations	0.03 Sec, 5
Under relaxation factor (Pressure)	0.4
Under relaxation factor (Velocity)	0.8
Under relaxation factor (Segregated VOF)	0.8

5.3.2.8 Visualizing the wave pattern and propagation of the free water surface

An iso surface is created for the volume fraction of water at a value of 0.5 (50% water, 50% air) ([section 4.5.4](#)). Therefore it gives the position of the water- air- interface corresponding to the free surface. In a scalar scene by selecting the derived isosurface the wave pattern can be visualized. The free surface can be plotted at the free water surface to get a good visual representation of the effect of the hull resistance on the surrounding water.

5.3.3 Grid convergence study (Fn 0.22)

Table 15 shows predicted resistance at various grids. The variation of total resistance coefficient C_T is not monotonic. The largest difference related to measured value is obtained on medium grid. While the friction drag reduces monotonically with grid refinement the pressure drag is largest medium grid. It is usual that such variation is observed when using unstructured locally refined grid (Enger et al). 8 million cells if used with proper local refinement can predict acceptable results for the parameters considered as shown thus increasing the computational efficiency. However based on various experiments done at CTO S.A (Bugalski et al) it was decided to use more number of cells to predict accurate wave field and wake.

Table 15: Grid convergence study

Mesh type	No.cells	C_T	C_F	C_P	Trim	Sinkage
	Million	$\times 10^{-3}$	$\times 10^{-3}$	$\times 10^{-3}$	(°)	m
Mesh1	18.18	4.891	3.188	1.703	0.0935	0.0113
%Diff		-2.34			17.5	-2.7
Mesh2	11.64	4.943	3.224	1.726	0.093	0.0113
%Diff		3.497			17.9	-1.18
Mesh3	7.91	4.95	3.23	1.713	0.094	0.0112
%Diff		3.358			17.07	-1.81

5.3.4 EFD vs CFD comparison for resistance and motion

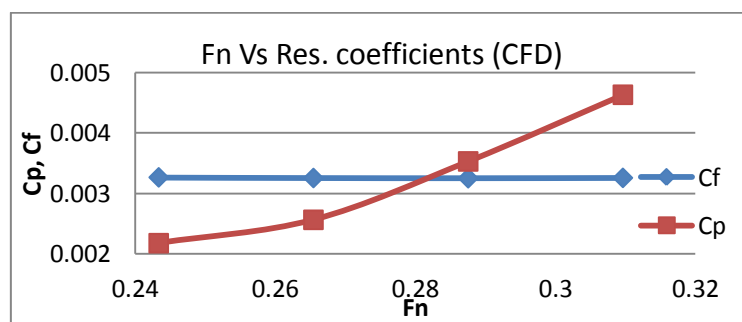


Figure 20: Froude number vs Resistance

It is interesting to note that the contribution of pressure drag to total resistance increases sharply with increasing Froude number where as frictional drag is almost steady.

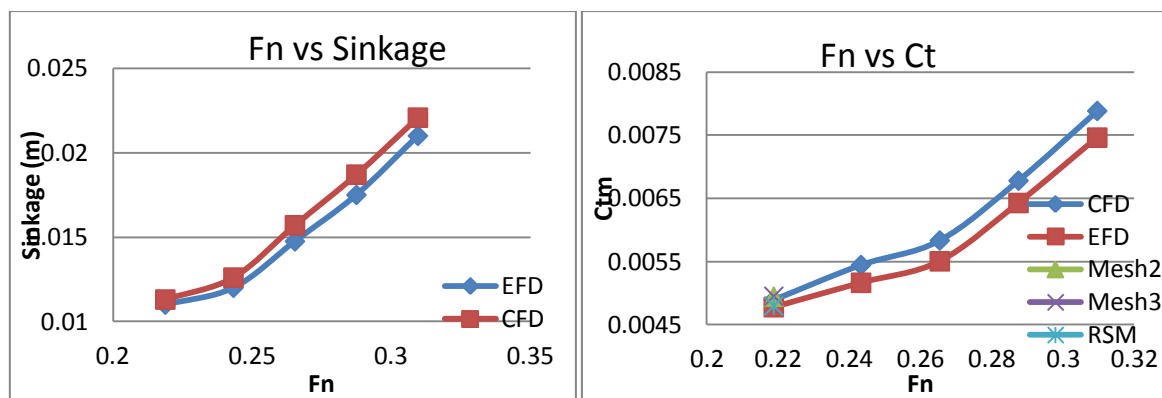


Figure 21 Fig (L) Froude number vs sinkage, fig (R): Froude number vs Total resistance

The results in table 16 shows good agreement with experiments except trim value that needs investigation and is not plotted. The error percentage of total drag coefficient increases from 2.3 to 5.3 % with increasing Froude number. Attention has to be paid to this behavior and a similar trend is found by [\(Enger et al\)](#).

Table 16: Resistance test results

	Fn	RN_M	C_{TM}	C_p	C_F	Trim	Sinkage
		$\times 10^6$	$\times 10^{-3}$	$\times 10^{-3}$	$\times 10^{-3}$	($^\circ$)	(m)
	0.2188	7.5	4.891	1.703	3.188	0.0935	0.0113
%Diff EFD			2.34			17.5	-2.7
	0.2433	8.304	5.445	2.178	3.267	0.114	0.0126
%Diff EFD			5.18			11.5	-5
	0.2654	9.0589	5.834	2.565	3.256	0.128	0.0157
%Diff EFD			5.655			19.86	-6.4
	0.2875	9.8138	6.781	3.53	3.253	0.115	0.0187
%Diff EFD			5.22			28	-6.8
	0.3096	10.569	7.885	4.632	3.258	0.052	0.02208
%Diff EFD			5.36			49	-5.14

% Diff EFD- Error percentage compared to experimental results determined with ITTC method.

5.3.5 Effect of turbulence model on results

For this calculation the fine mesh was used. RSM model predicted the resistance coefficient close to the model test values but the trim and sinkage showed different behavior. It also performed well in the wake prediction when compared to others. RSM model consumed 30% more time for convergence for the same mesh and physics values as of K- ϵ model.

Table 17: Turbulence model comparison

Turbulence model	F_n	RN_M	R_{TM}	C_{TM}	Trim	Sinkage
		$\times 10^6$	N	$\times 10^{-3}$	($^\circ$)	M
RSM	0.2188	7.5	42.5	4.891	0.0935	0.0113
K- ϵ	0.2188	7.5	41.68	4.797	0.1	0.0117
%Diff (EFD vs K- ϵ)				2.33	17.5	-2.72
%Diff (EFD vs RSM)				0.5	11.8	-6.36

% Diff EFD - Error percentage with respect to experimental results determined with ITTC method.

5.3.6 Residuals and convergence analysis

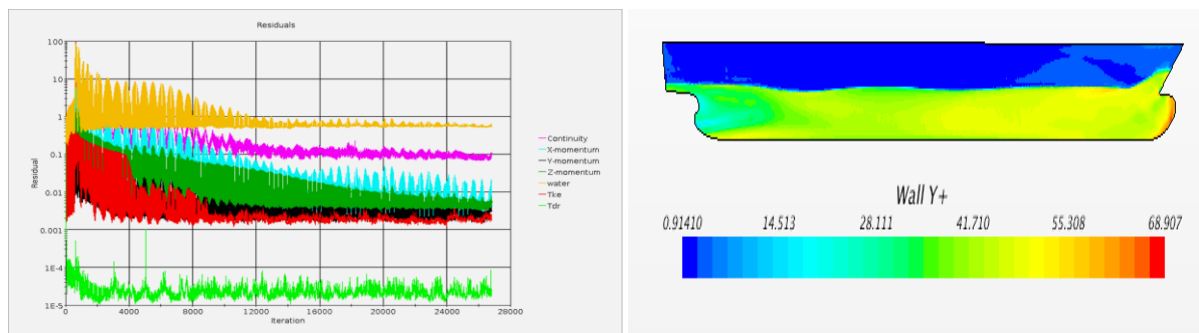


Figure 22: Fig (L) Residuals, Fig (R) Wall Y+ values

Based on the monitor plots a physical time of 60 seconds is required to have good convergence. Frictional resistance and sinkage converges faster than pressure resistance and trim values. A Y+ value less than 50 is targeted but it resulted in large number of iterations to achieve that nevertheless the value of 68 is acceptable for the test case and the results agreed to a wider range with the experimental data.

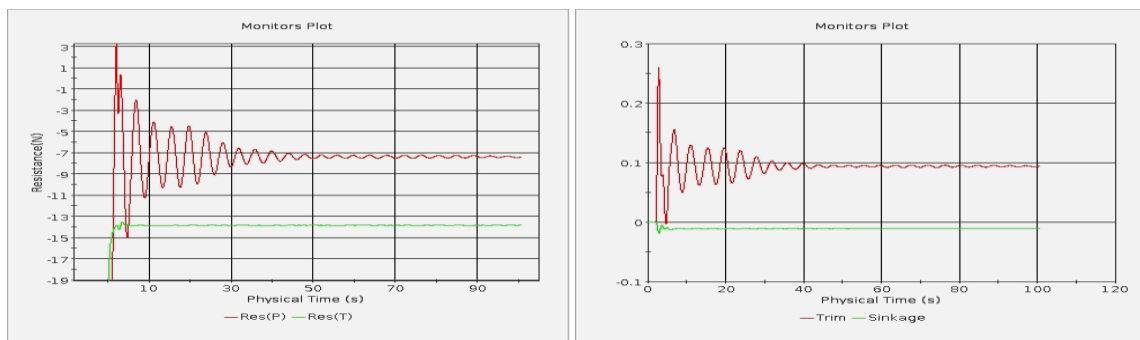


Figure 23: Monitor plot

5.3.7 Wave profile

This part is not directly related to the self propulsion tests nevertheless it is interesting to have an overview with various turbulence models, mesh parameters for the service speed. The

setup values and wave contours can be used as a reference for the future experiments aimed at hull optimization (3.4.1) if any implemented. Global wave patterns are shown in figures 24 and 25 since location wise results are not required in this stage and can be determined when needed.

5.3.8 Wave profile at service speed

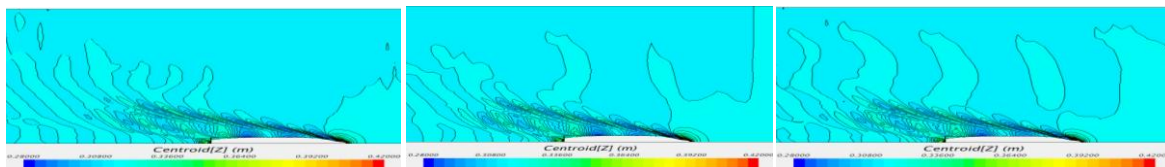


Figure 24: Wave profile Fig (L) Mesh 1, fig (c) Mesh2, fig (R)Mesh3

All three meshes as mentioned in figure 24 predicted the results with good agreement to each other.

5.3.9 Results obtained from mesh1

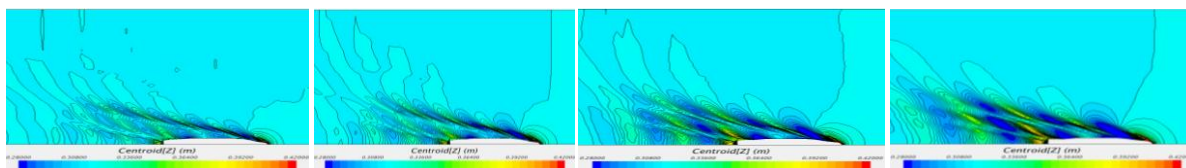


Figure 25: Wave profile for Fn 0.2433, 0.2654, 0.2875, 0.3096 respectively from left

The highest water elevation is always behind ship stern and the minimum water level is always at hull shoulder. Their order of magnitude grows with growing Froude number. But the exact location wise magnitude was not determined since it is not required for forthcoming experiments. However it is noteworthy to underline this behavior and a further investigation can be made.

5.3.10 Wake field predicted with various mesh and models

The wake is evaluated so that flow improvement devices can be incorporated in a later stage to improve the wake field (Table 6). Various turbulence models were tried out to figure out the most suitable one capable of predicting it accurately. Unfortunately experimental results were unavailable for accurate comparison. On the basis of an old test result (report hardcopy) general pattern is compared with the turbulence models. Reynold's stress model (RSM) predicted the hook shape, unique to wake field accurately than $K-\epsilon$ model. For three different types of mesh tried with $K-\epsilon$ model the wake field pattern improved by increasing the number

of cells. Earlier simulations carried out at CTO S.A ([Bugalski et al 2012](#)) revealed K- ϵ model is acceptable for the propulsion tests and wake prediction.

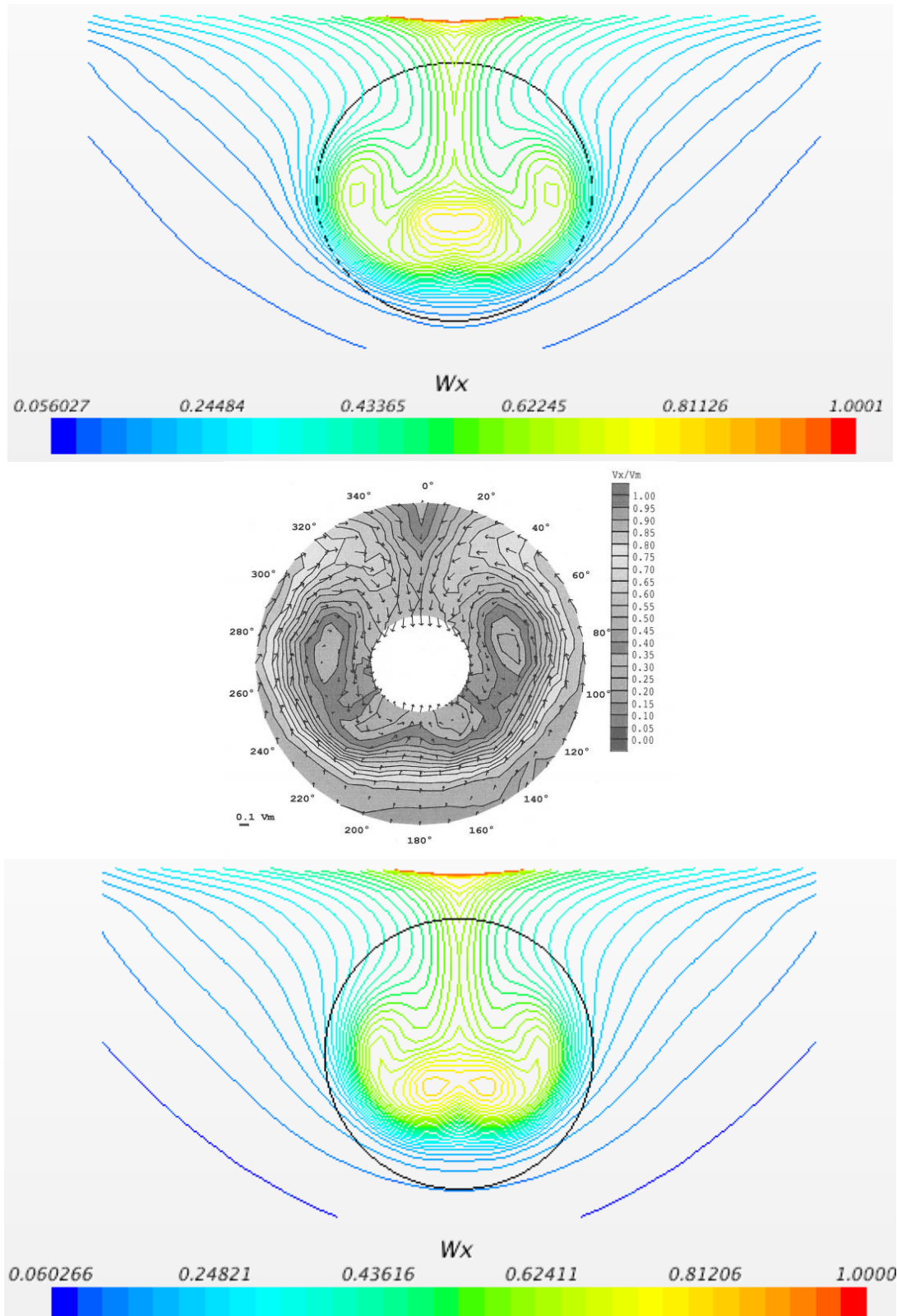


Figure 26: RSM Model (Top), Experiment results (Middle), K- ϵ Mesh 1(Bottom)

Master Thesis developed at West Pomeranian University of Technology, Szczecin

6 OPEN WATER TEST

The characteristics of a propeller is recorded in the open water test whereby it is unaffected by the wake and is utilized for further comparison when fixed in the ship.

6.1 Setup and test procedure

The open water experiment is conducted by towing the open water boat at a steady speed while running the propeller at a constant velocity rate (45). The speed of the boat (speed of advance V_A). The revolution rate n , thrust T and torque Q of the propeller are measured in each run. It is usual to run the model propeller to run at speeds of advance at a constant revolution rate. The speed of advance is varied in steps from zero to the value at which the propeller thrust just becomes negative. The measured thrust and torque are corrected for the idle thrust and torque i.e. when the experiment is carried out with a dummy boss of equal weight replacing the propeller.

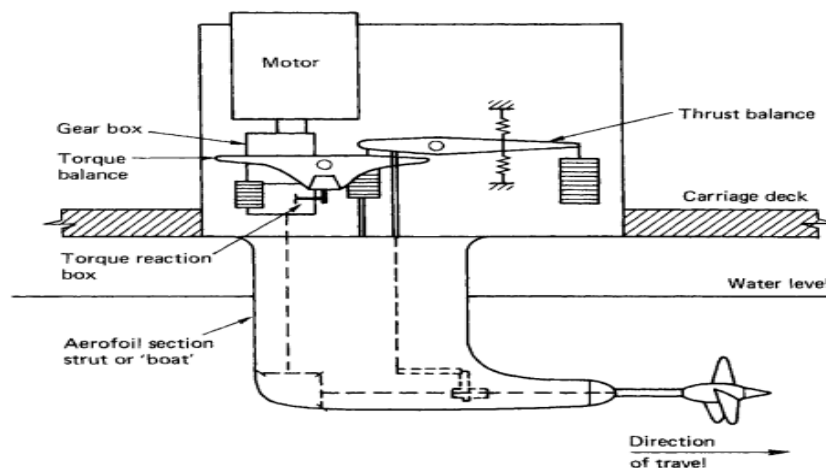


Figure 27: Experimental set up open water test (47)

The size of the model propeller being governed by the size of the ship model if it is intended to be used in the self propulsion test and the capacity of the dynamometer used. It should have a high Reynolds number to make the flow turbulent. As a further measure the surface roughness is increased to assist the turbulent flow. It is recommended that the model propeller Reynolds number based on the resultant of the axial and tangential velocities and the chord at $0.7R$ be at least 5×10^5 . For the open water experiment the model propeller is attached to a propeller dynamometer fitted in an "open water boat". The results are non-dimensionalised as follows (25):

Thrust coefficient K_T
$$\frac{T}{\rho D^4 n^2} \tag{17}$$

Torque coefficient K_Q
$$\frac{Q}{\rho D^5 n^2} \tag{18}$$

Advance coefficient J
$$\frac{V_A}{n \cdot D} \tag{19}$$

Reynold's number RN
$$\frac{C_{0.7}}{\nu} \sqrt{V_A^2 + (0.7\pi Dn)^2} \tag{20}$$

ν -Kinematic viscosity of water(m²/sec), $C_{0.7}$ -chord length of radius of 0.7, propeller diameter D , T - Thrust (N), Q - Torque (Nm), ρ - water density (kg/m³), V_A - advance velocity (m/sec).

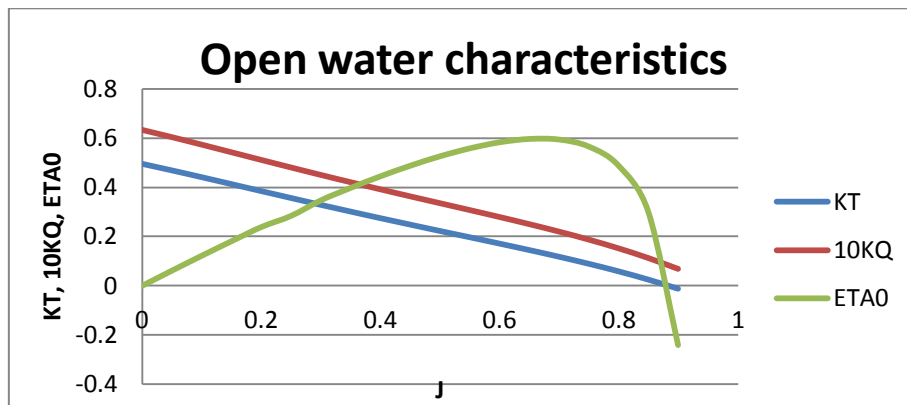


Figure 28: Open water characteristics of propeller1.

Table 18: Results of an open water test performed at CTO S.A with indigenously designed propeller.

Propeller1 specification		J	K_T	10 K_Q	η_0	$RN \times 10^{-6}$
No blades/ Rake/ Skew	4/0/20°					
NACA profile mean line	16/0.8	0	0.4945	0.6337	0	0.8436
Diameter (mm)	226	0.1	0.4404	0.5739	0.1221	0.8526
Pitch ratio at 0.7R (P/D)	0.942	0.2	0.3841	0.5119	0.2388	0.8574
Exp area ratio	0.673	0.3	0.3283	0.451	0.3475	0.8609
Hub ratio	0.3	0.4	0.2744	0.3926	0.4451	0.8654
Blade width at 0.7R (mm)	102.4	0.5	0.2225	0.3363	0.5266	0.8722
Propeller RPS (anticlockwise)	19	0.6	0.1713	0.2803	0.5835	0.8821
Tank water temperature (Deg C)	15.2	0.7	0.118	0.221	0.5949	0.8948
Sp.Density (Kg/m ³)	999	0.8	0.0588	0.1531	0.4888	0.9094
Kinematic viscosity [10E-6(m ² /sec)]	1.133	0.9	-0.0117	0.0697	-0.2416	0.9243

7 OPEN WATER TEST STAR-CCM+

The open water tests were performed in the following steps:

- Validating the numerical tests for the propeller1 (table 18) with experimental results.
- Performing a test for propeller2 which is enlarged by 15% keeping other ratios same.

7.1 Procedure

The circular computational domain is created around the propeller and a rotating reference frame is created around it. The circular domain diameter $4D$, length forward $5D$ and backward extended up to $3D$ where D is the diameter of the propeller. Coordination system is chosen in the centre of the blade. The prism layer thickness and mesh base size were together modified by trial to have a Y^+ value near about 50 as suggested by ITTC (24).

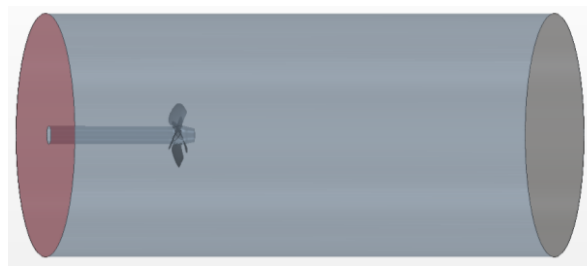


Figure 29: Computational domain

7.1.1 Meshing

Polyhedral mesh is utilized for this and its features are mentioned in [section 4.5.3](#). Prism layers were refined where required. Around the propeller for a region of diameter $4D$ the mesh is refined around the blades to have a finer mesh to get accurate results. The surface mesh at shaft is modelled with coarser mesh since this region is not significant for the results. The mesh parameters are mentioned in table 19.

Table 19: Mesh parameters

Mesh type	Surface remesher, Prism layer, Polyhedral
No cells used	2.8million(Propeller1), 4million(Propeller 2)
No. prism layers, stretching	4, 1.3
Prism layer thickness (m)	9E-4
Surface growth rate	1.3
Surface size	

Tet/Poly density (density and growth factor)	0.9,1.5
Blade surface mesh refinement	
Relative minimum , target size (m)	4.5E-4, 0.0036
Shaft mesh refinement (for coarser mesh)	
Relative minimum , target size (m)	4.5E-4, 0.0158
Mesh refinement in the domain boundary	Prism layer mesh is disabled

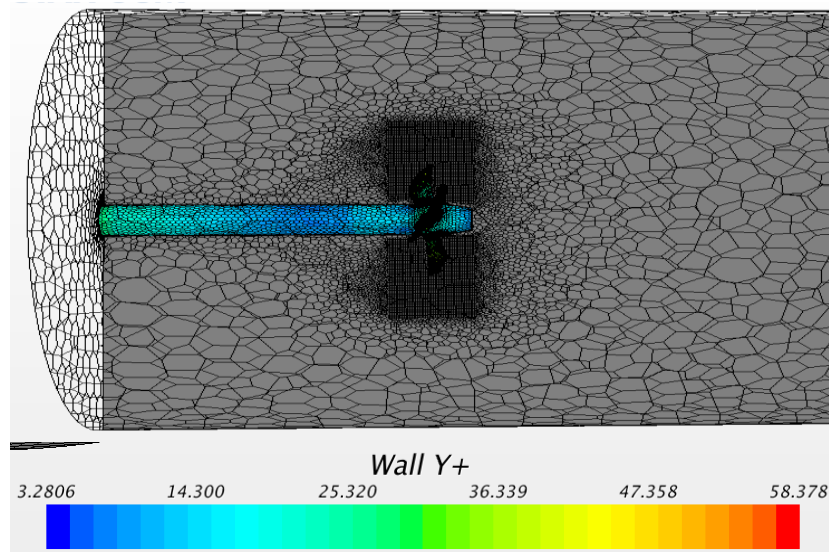


Figure 30: Mesh refinement and Wall Y+ values

7.1.2 Experimental setup

For open water calculations the propeller inflow is uniform so the moving reference approach is applied. The solver was running in steady mode and the rotation of propeller is accounted by the moving reference frame (4.5.5) approach. Turbulence model Realizable K- ϵ is used. This approach is valid in open water where the propeller experiences a completely uniform inflow field. Water density, viscosity and Reynold's number were chosen to match the experimental values.

Table 20: Experimental setup

Physics: Constant density, Gradients, Implicit steady, K Epsilon turbulence, Liquid, Realizable K Epsilon two layer, RANS, Segregated flow, Two- Layer All Y+ wall treatment.
Motion specification: Rotating reference frame around stationary propeller.
Inlet & domain: Slip condition is imposed in the inlet and domain boundary.
Outlet: Pressure outlet with out prism layer.

7.1.3 Methodology

Thrust coefficient K_T torque coefficient K_Q and the open water efficiency η_0 are calculated for each value of J and are plotted in the propeller performance plot for comparison. The velocity of the flow V_A at inlet is defined as an initial condition in the domain. The velocity is driven by the advanced coefficient $J = \frac{V_A}{n \cdot D}$. (V_A - advance velocity, n - rate of revolution, D - propeller diameter)

In this steady simulation the value of J are defined by two field functions i and J . The field function i specifies the iteration on which the value of J changes (12). The starting value of J 0.2 is used because the aim was to detect the coefficients in the operating range decided. The value of J increases by 0.2 every 1800 iterations (decided upon the preliminary iterations corresponding to good convergence). After defining the field function this was made as an input as the initial velocity for the fluid domain. The rotation of the propeller is modeled using moving reference frame. The simulation is run for a range of advance coefficients J ranging from 0.2-0.8.

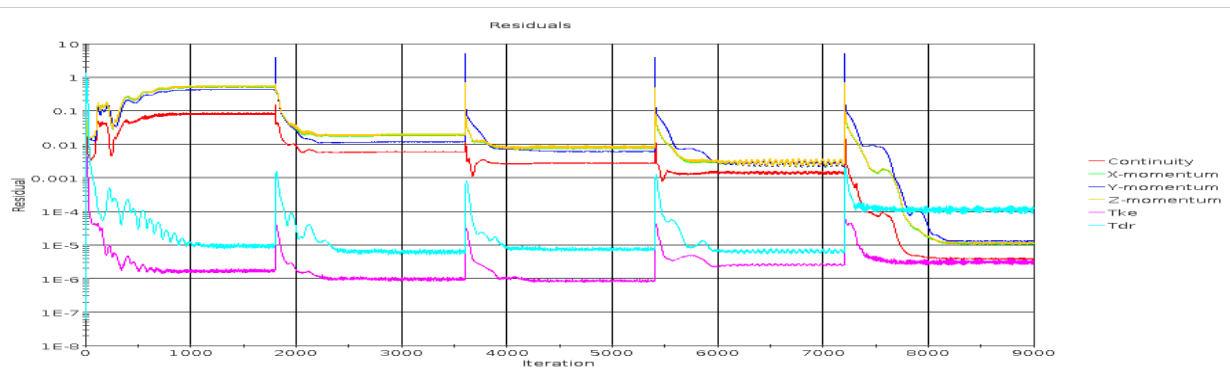


Figure 31: Residuals for propeller 1

Table 21: Propeller specification

	Propeller 1	Propeller 2
No blades	4	4
Diameter (m)	0.226	0.2599
Pitch ratio at 0.7R	0.942	0.942
Expanded area ratio	0.673	0.673
Hub ratio	0.3	0.3
Blade width at 0.7R(m)	0.1024	0.1024
Propeller RPS	19	19

Table 22: Results

EFD					CFD					
Propeller1					Propeller 1*				Propeller 2*	
J	KT	10KQ	ETA0	Rn (x10E-6)	KT	% Diff	10KQ	% Diff	KT	10KQ
0.2	0.384	0.5119	0.238	0.8574	0.386	-0.63	0.54	-5.3	0.390	0.54
0.4	0.274	0.3926	0.445	0.8654	0.274	-0.14	0.41	-5.3	0.276	0.41
0.6	0.171	0.2803	0.583	0.8821	0.169	1.2	0.29	-5.7	0.169	0.29
0.8	0.058	0.1531	0.488	0.9094	0.061	-2.7	0.168	-10.0	0.060	0.16
No of cells used					2.8 million				4 million	

*Propeller 1 designed at CTO S.A (Table 18). Propeller2: 15% enlarged size of propeller1 with other ratios similar to propeller 1.

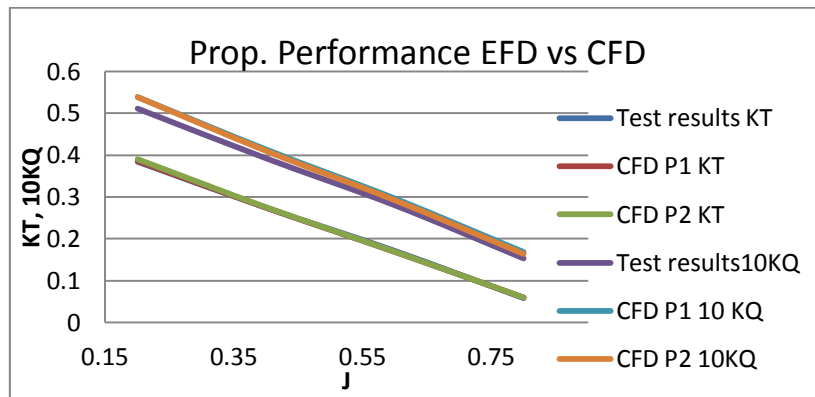


Figure 32: Propeller performance EFD vs CFD

Remarks

Simplified meshing used resulted in more number of cells and computational cost. If the region is divided into static (region around shaft and the fluid domain) and rotating (domain around propeller) and if extruder meshing done around the shaft the computation can be optimized (12).

7.2 Results

- Change in propeller diameter does not influence much in the parameters.
- Results have a very good agreement with the experimental results for the K_T values in operating range considered, but K_Q values differ to an extent and needs investigation.
- It was ensured that Propeller2 characteristics doesn't change much when compared to that of propeller1 and experimental coefficients of the later can be used in analyzing self propulsion tests. Experimental values are more reliable (proven in ship's trial) in this case since there are some discrepancy in CFD vs EFD results.

8 SELF PROPULSION TEST

Self propulsion experiments are performed to determine the performance of the ship hull and propeller taken together. An analysis of a self propulsion experiment allows one to predict the delivered power and the rate of revolution of the ship propeller at a given speed of the ship and to determine the wake fraction, thrust deduction fraction and relative rotative efficiency.

8.1 Procedure

The model propeller is fitted in its position stern of the ship model and connected to a dynamometer for measuring the thrust and torque of the propeller at various revolution rates. The ship model should be fitted with all appendages as far as possible particularly those lying in the propeller slipstream (45). The ship model is attached to a resistance dynamometer which measures the force required to make the ship model move at a constant speed with the propeller running. The ship model is ensured that it floats at the correct waterline and towed at a steady speed with the propeller running at constant RPM, thrust and torque of the propeller. The force applied to the ship model through resistance dynamometer are measured.

8.1.1 Towing force

The towing force is applied to the model during the test to correct the wrong Reynold's number in model scale as it is impossible to scale correctly both with respect to Froude and Reynold's number (45). The analysis of the data recorded in a self propulsion experiment when a ship is moving at a steady speed V_S with its propeller producing thrust T_S ,

$$R_{TS} = (1 - t)T_S \quad (21)$$

Where R_{TS} is the resistance of the ship at the speed V_S and t the thrust deduction fraction. With model scale λ , and D_M and D_S as model and ship propeller diameters, model speed V_M according to Froude similarity it can be shown that:

$$D_S = \lambda D_M \quad V_M = V_S \lambda^{-0.5} \quad (22)$$

During self propulsion tests at speed V_M the model propeller runs at a revolution n_M and has a thrust T_M and torque Q_M while the force applied through resistance dynamometer is F then

$$F = R_{TM} - (1 - t)T_M \quad (23)$$

R_{TM} being the resistance of the model at the speed V_M . This may be written as:

$$F = R_{TM} - (1 - t)K_{TBM}D_M^5 n_M^2 \rho_M \quad (24)$$

Where K_{TBM} is the thrust coefficient of the model propeller in the behind condition and ρ_M is the density of the water in which the experiment is carried out. If the model propeller and the ship propeller are to fulfill the conditions of dynamic similarity then

$$J_S = J_M \quad K_{TBS} = K_{TBM} \quad w_S = w_M \quad (25)$$

where J_S and J_M are the advance coefficients of the ship propeller and the model propeller, w_S and w_M the corresponding wake fractions and K_{TBS} the thrust coefficient of the ship propeller in the behind condition. Using equations 21 and 22 with equation 25 one obtains:

$$n_M = n_S \lambda^{-0.5} \quad (26)$$

and then one may write equation 24 with the help of equations 21 and 22 as follows:

$$\begin{aligned} F &= R_{TM} - (1 - t)K_{TBS}D_S^4 n_S^2 \rho_S \left(\frac{n_M}{n_S}\right)^2 \left(\frac{D_M}{D_S}\right)^2 \\ &= R_{TM} - (1 - t)T_S \frac{\rho_M}{\rho_S} \lambda \lambda^{-4} \\ &= R_{TM} - \frac{\rho_M}{\rho_S} \frac{R_{TS}}{\lambda^3} \end{aligned} \quad (27)$$

In terms of the total resistance coefficients of the model and the ship this becomes:

$$\begin{aligned} &= C_{TM} \frac{1}{2} \rho_M S_M V_M^2 - (1 + x)C_{TS} \frac{1}{2} \rho_M S_M V_M^2 \frac{S_S}{S_M} \left(\frac{V_S}{V_M}\right)^2 \frac{1}{\lambda^3} \\ &= \frac{1}{2} \rho_M S_M V_M^2 C_{TM} - [C_{TM} - (1 + x)C_{TS}] \end{aligned} \quad (28)$$

Equations 27 and 28 show that for dynamic similarity as indicated by equation 25 the ship model is not fully self propelled and the thrust of the model propeller must be augmented by the force F applied through the resistance dynamometer. The condition represented by equation 27 or 28 is called "ship self propulsion point on the model".

8.1.2 Constant speed or British method

The set up is the same as for a resistance tow which means that the model is connected to a resistance dynamometer that measures the actual resistance during the test. The model speed

and desired propeller loading should be selected before each run and the corresponding propeller thrust should be estimated. The towing carriage then accelerates the model to the desired speed and simultaneously increases the propeller rate of revolutions so that desired thrust is reached closely after target speed is reached the measurement starts when the running conditions have settled.

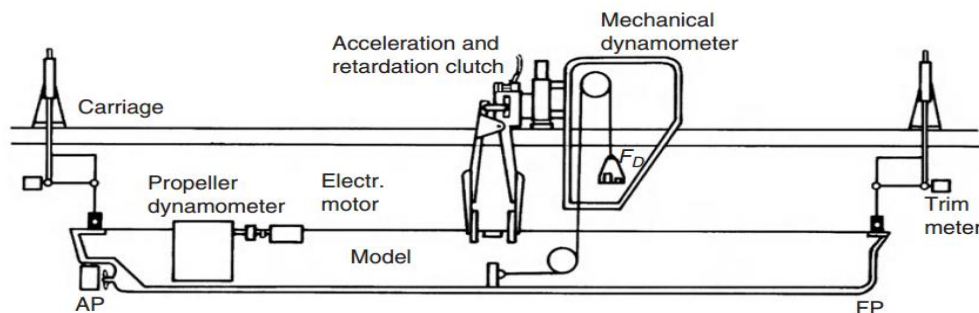


Figure 33: Experimental setup for self propulsion test (British method) (47)

Tests are carried out for several values of n_M at each value of V_M and F , T_M and Q_M are measured. This allows the data to be analysed for different load factors which may be selected after the experiment is over. In actual practice the constant method for different loadings and the constant speed method for different speeds are equivalent since both lead to values of F , T_M and Q_M as functions of V_M and n_M .

8.2 ITTC Recommended practice (2008b) for single screw ships.

The analysis of the data of a self propulsion experiment requires the resistance of the model and the resistance of the ship derived from it as well as the open water characteristics of the model propeller obtained through the open water experiment (26). The resistance of the model should be corrected between the model resistance data for any temperature difference between the resistance experiment and the self propulsion experiment. For each model speed V_M and the corresponding ship speed V_S the required force F is determined from the model tests R_{TM} and the ship resistance R_{TS} using equation 27. The model propeller revolution rate n_M for this value of F and the corresponding values of T_M and Q_M are then obtained.

8.2.1 Thrust and torque coefficients

Values of T_M , n_M and Q_M at the ship propulsion point on the model for the speed V_M are converted to the thrust and torque coefficients, K_{TBM} and K_{QBM} .

$$K_{TBM} = \frac{T_M}{\rho_M D_M^4 n_M^2} \quad K_{QBM} = \frac{Q_M}{\rho_M D_M^5 n_M^2} \quad (29)$$

With open water characteristics of the model propeller (K_{TBM} , K_{QBM} and η_O as functions of J)

(a) J , K_{QM} and η_O for $K_{TM} = K_{TBM}$ can be found based on thrust identity ([figure 39](#)).

(b) (a) J , K_{TM} and η_O for $K_{QM} = K_{QBM}$ can be found based on torque identity.

8.2.2 wake fraction (w)

Using equation 30 by means of open water diagram and using K_{TM} (from self propulsion test) as input data and reading of K_{TM} and K_{QBM} (open water test) by thrust identity the fraction is,

$$w = 1 - \frac{J n_M V_M}{D_M} \quad (30)$$

To find thrust deduction factor, skin friction correction force, results from resistance test and the calculated thrust from the self propulsion test are used and formulated as

$$t = 1 - \frac{R_{TM} - F_D}{T_M} \quad (31)$$

8.2.3 Rotative efficiency

$$\eta_{RT} = \frac{K_{QOM}}{K_{QM}} (\text{Thrust identity or torque identity}) \quad (32)$$

8.2.4 Hull efficiency

The two quantities in equations 30, 31 is now combined together in the hull efficiency η_H . This parameter expresses the difference between delivered power and effective thrust.

$$\eta_H = \frac{1 - t}{1 - w} \quad (33)$$

8.2.5 Open water efficiency

$$\eta_{OTM} = \frac{J_{TM} K_{TM}}{2\pi K_{QOM}} \quad (34)$$

8.2.6 propulsive efficiency

$$\eta_D = \eta_O \eta_R \eta_H \quad (35)$$

8.3 Self propulsion experiments at CTO S.A

Experiments in model scale were carried out in the towing tank facility at CTO S.A. in the year 2005 by means of British method. Additional towing force taking into account the difference between Reynold's number of ship and model, assumed resistance increase in service conditions is determined as skin friction correction , $F_D = 0.5 \rho_M v_M^2 S_M (C_{TM} - C_{TS})$.

Table 23: Results for the self propulsion experiments at CTO S.A

Ship data					Test Data				
Length of water line		$L_{WL}(m)$		55.13	Scale factor		1	10	
L_{PP}	54.13m	B	10.5m	T	3.15m	Water properties		Full scale	Tank
Appendages		None			Temperature		T(°C)		
Draught		$T_F, T_A(m)$		3.15,3.2	Mass density		P(kg/(m ³))	1025.9	998.5
Displacement		$\nabla (m^3)$		1127	Kinematic viscosity		10 ⁻⁶ m ² /sec	1.188	1.060
Wetted surface		S (m ²)		672	Propeller data (Propeller1)				
Form factor		K		0.1	No . propellers		1	No. Blades	4
Hull roughness		$K_S (10^{-6}m)$		150	Diameter		D(m)	2.260	
Roughness allowance		$\Delta C_F (10^{-3})$		0.826	Pitch ratio at 0.7R		P/D	0.942	
Air res. coefficient		$C_{AA} (10^{-3})$		0.109	Roughness		$\rho_S(10^{-6}m)$	30	

Values for model							
V_S (Knots)	V_M m/sec	R_{TM} (N)	F_D (N)	n_M (Rps)	T_M (N)	Q_M (Nm)	Fn
9.0	1.464	33.2	3.38	7.9	38.81	1.259	0.1991
9.5	1.545	37.7	3.62	8.51	45.08	1.511	0.2102
10	1.627	42.62	3.86	9.12	52.34	1.746	0.2213
Model							
V_S (Knots)	$V_M(m/sec)$	t	$w_M (x 10^{-3})$	$\eta_{HM} x 10^8$	$\eta_R (x 10^{-3})$	$J_M (x 10^{-3})$	η_{OM}
9.0	1.464	0.232	0.428	1.344	1.034	0.469	0.503
9.5	1.545	0.244	0.417	1.296	1.000	0.468	0.502
10	1.627	0.260	0.414	1.264	1.002	0.463	0.498

9 SELF PROPULSION TESTS STAR-CCM+

Self propulsion tests were carried out numerically in the following steps:

- Performing a self propulsion test in a model scale of the ship with rudder to validate the simulation against experiments.
- Removal of rudder and relocating the propeller1 aft in three different locations and performing self propulsion tests at each of these positions.
- Repeating the tests with a propeller2 with the same locations as in the above step.

9.1 Introduction

Computations of flow around the ship hull with rotating propeller in propulsion tests have an unsteady character and therefore needs more time for convergence. The model is complex in nature because of the mutual interaction between hull, propeller and rudder. The simulation must be run in transient mode i.e. time accurate. In this test dynamic trim and sinkage of the hulls were neglected, propeller operation was modeled. The numerical simulation is done in the model scale with a rotating propeller and considering the free surface to predict the hull propeller interaction effects. The sliding mesh model as described in section (4.5.5) is utilized to implement the propeller rotation.

9.2 Procedure

9.2.1 The computational model

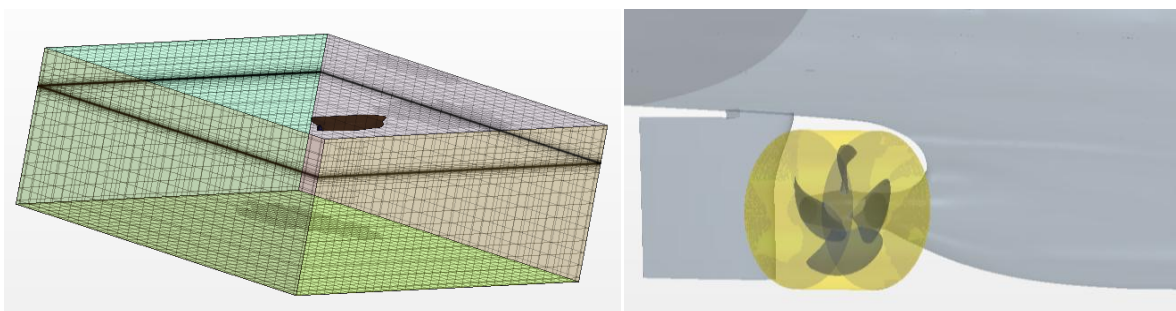


Figure 34: Fig (L): Computational domain Fig (R) Sliding interface around propeller

The numerical tank is modeled in to two regions namely propeller and tank domain respectively. The former is a region around the propeller and the later includes the bulk of the liquid, hull and boundary regions of the domain. The domain extended $0.5L$ top, L forward and bottom, $2L$ aft, port and star board where L is the length between perpendiculars. An interface of $1.2D$ (D is the diameter of the propeller) separates both the region.

The grid in the propeller region rotates around the stationary propeller. The grid in the tank remains stationary (not rotating). The two grids slide past each other at a cylindrical interface. In the tank region the standard conservation equations for mass and momentum are solved (9). In the sliding mesh model motions of the propeller region is accounted by a grid motion of the propeller domain and the flow variables are interpolated across the sliding interface. In this unsteady problem all interaction effects can be determined accurately. The computations were carried out for a model speed corresponding to $F_n = 0.22$ and $RN_M = 8.37 \times 10^6$.

9.2.2 Mesh1 (Propeller)

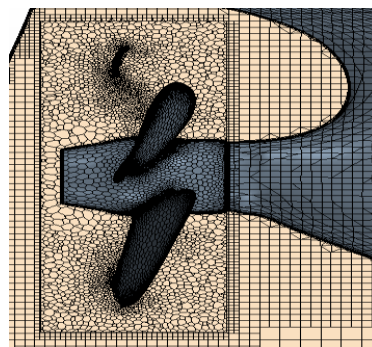


Figure 35: (Mesh in propeller region)

Polyhedral mesh is used with prism layers and surface remesher option. Around the propeller a rotating domain is created and connected to the computational domain by an interface namely sliding grid approach. Polyhedral mesh provide a balanced solution for complex mesh generation problems. They are relatively easy and efficient to build requiring no more surface preparation than the equivalent tetrahedral mesh. They also contain approximately five times fewer cells than a tetrahedral mesh for a given starting surface (12). Polyhedral meshing model utilizes an arbitrary polyhedral cell shape in order to create the polyhedral mesh from an underlying tetrahedral mesh which is automatically created as a part of the process. Mesh parameters can be found in table 24.

Table 24: Mesh1 (Propeller domain)

Mesh type	polyhedral mesher ,surface remesher, prism layer.
Cells used	0.99 million
No prism layers, Prism layer stretching	4,1.3
Prism layer thickness	0.00174m
Surface growth rate	1.35
Surface size refinement (Rel min/ target size)	0.044m, 0.175m.

Tet/Poly density (density and growth factor for tetrahedral and polyhedral mesher)	0,9,1,5
--	---------

9.2.3 Mesh2 (Domain and hull)

Trimmed mesher is utilized in the computational domain. This type of mesh provides a robust and efficient method of producing a high quality grid for both simple and complex mesh generation problems. They are basically hexahedral mesh with minimum skewness. This type of mesh is very efficient to refine the cells in a wake region around the propeller.

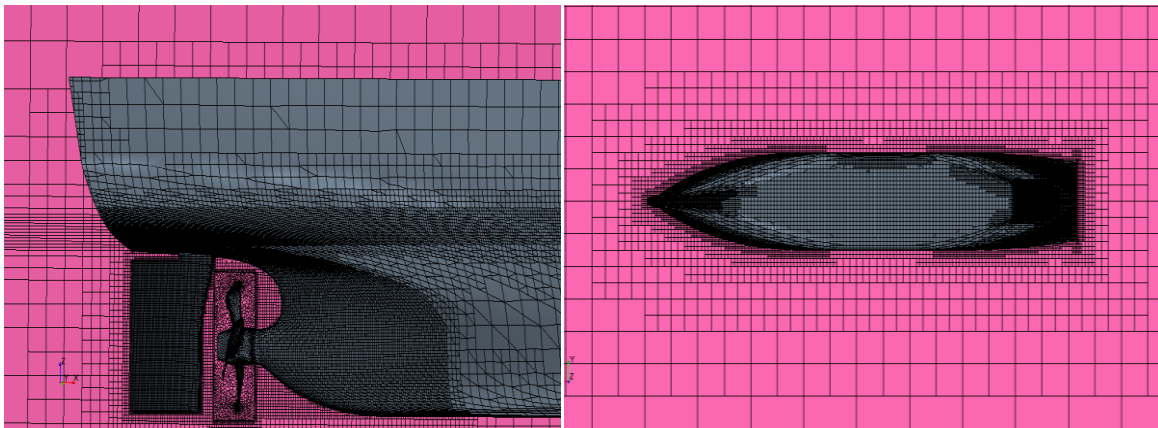


Figure 36: Fig (L) & Fig (R) Mesh refinement in various zones

As shown above local refinements were done near free surface and in region aft of the ship where flow separation takes place. Around the hull a no slip condition is imposed and four layers of prism layers are used.

Table 25: Computational domain

Mesh type	Trimmer, prism layer, surface remesher.
Cells used	1.15 million
No prism layers, Prism layer stretching	4,1.3
Prism layer thickness	0.0017499 m
Surface growth rate	1.5
Surface size	
Relative minimum/ target size.	0.04375m, 0.175m.
Volumetric controls1 (free surface)	Trimmer anisotropic size relative to Z.
Volumetric controls2 (Aft near propeller)	Surface remesher relative to Z.
Volumetric controls3 (domain)	Trimmer isotropic size relative to Z.
Surface mesh refinement	Hull, rudder, inlet, outlet, side and top walls.

9.2.4 Boundary definition

Slip condition is imposed in the side, top, and bottom walls and also prism layer is disabled in this region. In the hull, rudder and propeller default prism layer parameters.

Table 26: Boundary definition

Boundary Name	Boundary Type
Tank Inlet	Velocity Inlet
Tank Outlet	Pressure Outlet
Tank Side, top	Wall (with slip condition)

9.2.5 Defining VOF wave and initial condition

The set up is similar as applied in resistance test section [6.3.2](#).

9.2.6 Selecting the Physics Models

The model is complex in nature because of the mutual interaction between hull, propeller and rudder. Computations of flow around the ship hull with rotating propeller simulating propulsion tests have an unsteady character and therefore need more time to obtain convergence so implicit unsteady model with Realizable K Epsilon two layer turbulence model has been chosen [\(8\)](#). The other parameters are constant density, Gradients, segregated flow, Two- Layer All Y+ wall treatment, VOF waves, segregated fluid isothermal.

9.2.7 Setting solver parameters and stopping criteria

Propulsion test is a transient simulation for which the appropriate time step, the number of inner iterations per time step are important. The required time step of 200 time steps per period as mentioned by [Vissonneau et al \(14\)](#) is required. But according to the simulations performed earlier at CTO S.A a 10 times larger time steps is sufficient to compare the two models and the same is applied for this simulations. The under relaxation factors according to table 27 are set to enhance the convergence per time step.

Table 27: Solver setup

Time step required/ used	0.0005sec, 0.005 sec
Under relaxation factor (Pressure)	0.3
Under relaxation factor (Velocity)	0.7
Under relaxation factor (Segregated VOF)	0.9

9.2.8 External towing force

The simulation is started by applying the same revolutions of the propeller corresponding to the service speed in which self propulsion experiments were carried out in the model scale (table 23). The friction correction force is evaluated by selecting a force monitor including the propeller blade, boss, rudder and hull. The resultant force gives the additional friction correction force that is applied to the model. Coefficients of thrust and torque were calculated after convergence and compared with the experimental results in a similar method demonstrated at Gothenburg workshop 2010 (30).

9.2.9 Convergence analysis

The results in figure 38 show that a physical time of 30 seconds (24 hours) can be considered for getting an appropriate convergence and for the forthcoming simulations this time interval was chosen as a stopping criteria because of the time constraints involved in the project.

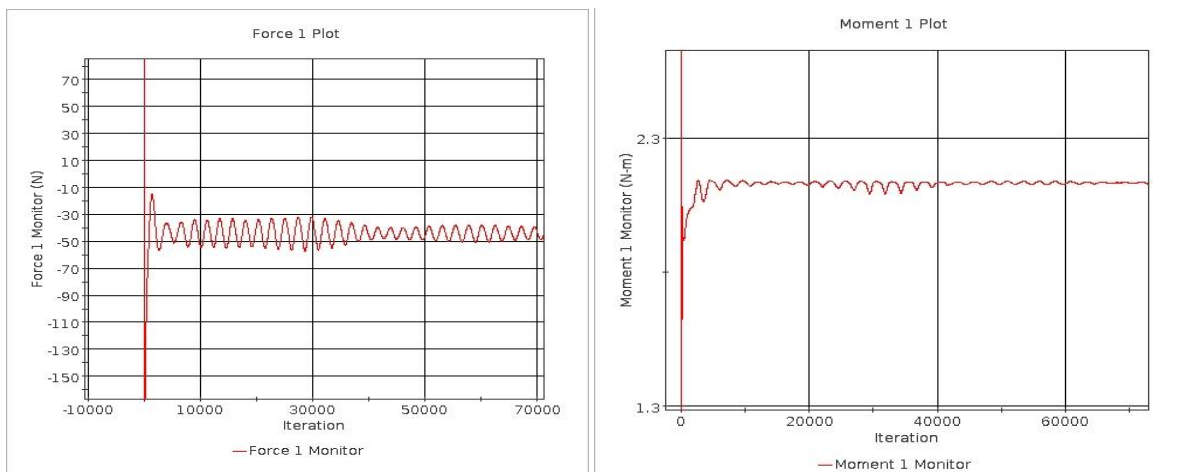


Figure 37: Monitor plots Fig (L) Resistance, Fig (R) Torque

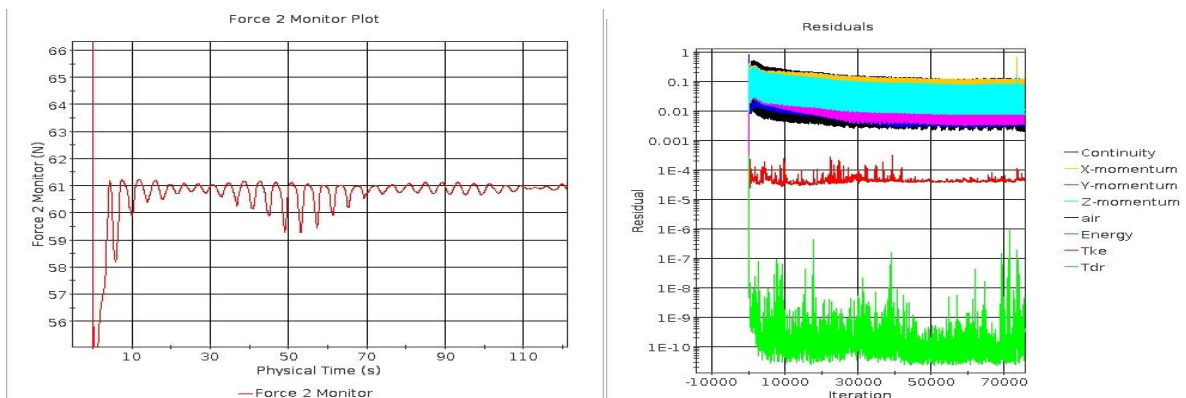


Figure 38: Fig (L) Thrust monitor plot, Fig (R) Residuals

9.3 Analysis

Table 28: EFD vs CFD results

	Experiments	STAR- CCM+	Error%*
Diameter(m)	0.226		
Seed(m/sec)	1.609		
Rps	8.99		
SFC (N)	3.81	3.50	8
Thrust (N)	50.67	42.00	16.12
Torque (N.m)	1.70	1.53	8.02
Resistance (N)	-	41.5	
C_P	-	0.00311	-
C_F	-	0.001613	-
K_T	0.24	0.20	
K_Q	0.04	0.03	
Delivered power (Watts)	95.78	86.40	

*Error percentage calculated as $\left(\frac{Ref-Com}{Ref}\right) \times 100$ where Ref is the experimental data taken as reference and Com is the value compared which is the Star-CCM+ results.

The results in table 28 shows a 8% difference of friction correction force (SFC) and thrust. But torque showed a considerable difference. This may be because of higher chosen time step. Ideally a time step of 2radians / seconds is used in the simulations concerned with rotational motions (Visonneau et al). But in this test a 10 times larger time step because of the computational and time restrictions involved since simulations were performed in a Pentium i5 processor not in cluster. Nevertheless the aim was to compare the self propulsion results of various cases. Based on similar tests performed in Ship Design and Research Centre (CTO S.A.) it was found that this error percentage is acceptable for comparing the various models and cases.

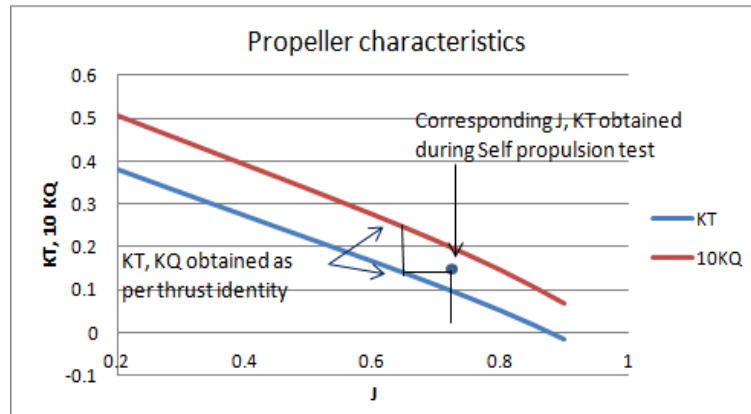


Figure 39: Example of thrust identity method

9.4 Results

- Friction correction force (SFC), K_T and K_Q are validated with experiments.
- Differences are within acceptable values and is valid for comparing cases as mentioned earlier.
- The corresponding skin friction correction obtained (with error) in the tests is the reference for the forthcoming experiments.
- The mesh and physical parameters can be retained.

10 PROPELLER RELOCATION

The rudder is removed from the ship for the experiments and the propeller is relocated axially aft to two different positions just before the stern similar to [knutsson et al.](#) At each position self propulsion tests were carried out with three set of RPM and based on this the results were interpolated for the skin friction correction (SFC) as obtained in the numerical self propulsion initially done with rudder. The obtained results for this condition were then corrected for the error percentage compared to experiments.

10.1 Case 1

The rudder has been removed and the propeller shifted aft to two different locations as shown. Propeller1 is used in this simulation.

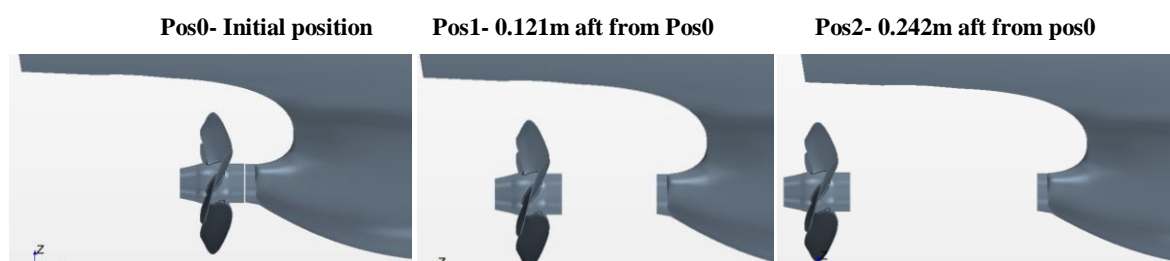


Figure 40: Fig (L)Position 0, Fig (C) Position 1, Fig (R) Position 2

Table 29: Case1 Results

	Pos 0		Pos 1			Pos 2		
Diameter (m)	0.226							
Rps	9.4	8	9.5	9.8	9.4	9.8	7.9	9.42
SFC (N)	4.8	21.1	3.5	-0.71	4.8	-0.6	22	4.8
Thrust (N)	49.4	29.8	51	55.85	42.5	48.4	20.6	39.65
Torque (N.m)	1.8	1.163	1.85	2.005	1.655	1.85	0.953	1.595
Resistance (N)	54.5	51	55	55	46.5	47	43	45

The linear behavior of RPS vs skin friction in figure 41 found to be linear which justifies the interpolation method employed in this simulation for the appropriate skin friction force with respect to the revolution.

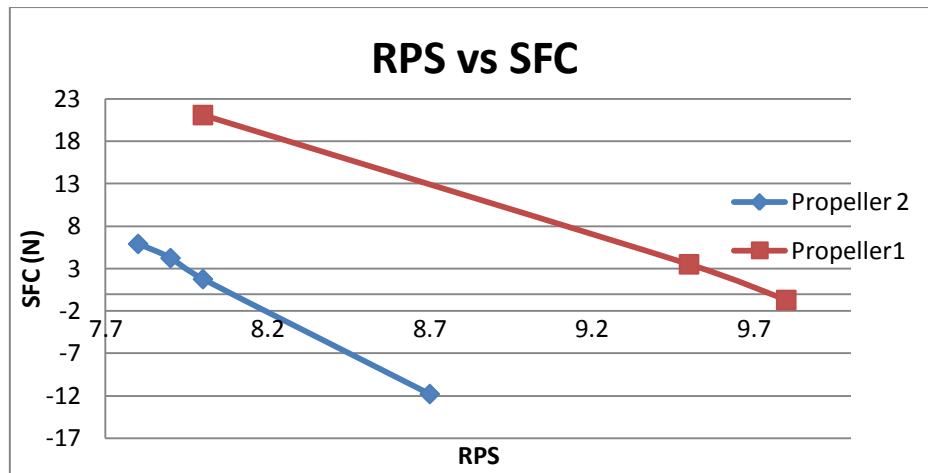


Figure 41: RPS vs SFC behavior

Table 30: Interpolated for the error percentage of SFC

	Error %	Pos0	Pos1	Pos2
Diameter (m)		0.226		
Rps		9.51	9.496	9.535
SFC (N)	8	3.81	3.81	3.81
Thrust (N)	8.85	60.75	52.35	48.979
Torque (N.m)	19.2	2.012	1.85	1.78
K_T		0.26	0.222	0.207
K_Q		0.038	0.0348	0.0334
Delivered Power (Watts)		120.25	110.395	107.04
Thrust deduction (t)		0.38	0.280	0.231
K_{QOM}		0.038	0.0335	0.032
J		0.75	0.75	0.75
J_{TM}		0.465	0.51	0.53
W_{TM}		0.381	0.32	0.29
Open water efficiency (η_{OTM})		0.51	0.54	0.545
Hull efficiency (η_{HM})		0.998	1.058	1.084
Rotative efficiency (η_{RT})		0.99	0.961	0.958
Propulsive efficiency (η_D)		0.504	0.549	0.566

* Values determined based on thrust identity

10.2 Case 2

The propeller diameter was enlarged 15% keeping other ratios constant and again tested for all the three positions as done in case1. Propeller2 is used in this test, same mesh parameters and physics values were retained during this process.

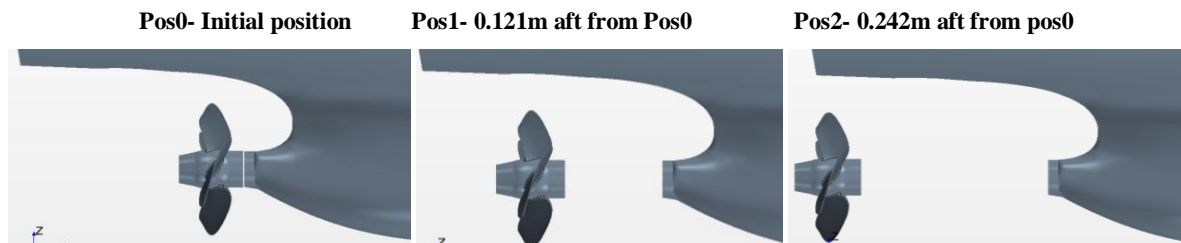


Figure 42: Fig (L)Position 0, Fig (C) Position 1, Fig (R) Position 2

Table 31. Case2 results

	Pos 0			Pos 1		Pos 2		
Diameter (m)	0.2599			0.2599		0.2599		
Rps	7.9	8.2	7.943	8	9.4	7.8	7.9	8
SFC (N)	4.5	-1.3	2.9	2.3	4.8	5.9	4.23	1.75
Thrust (N)	52	58.8	51.75	46.25	42.5	39.25	41.3	43.3
Torque (N.m)	2.29	2.55	2.31	2.18	1.655	1.955	2.035	2.11
Resistance (N)	56.5	57.8	54.5	47.4	46.5	45.5	45.5	45.5

Table 32: Interpolated for the error percentage

	Error %	Pos0	Pos1	Pos2
Diameter (m)		0.2599		
Rps		7.95	7.93	7.943
SFC (N)		3.81	3.81	3.81
Thrust (N)	8.85	63.38	53.39	50.298
Torque (N.m)	19.2	2.538	2.31	2.25
Resistance (N)	8.71	41.49	41.49	41.49
K_T		0.22	0.186	0.175
K_Q		0.0339	0.031	0.03
Delivered Power (Watts)		126.81	115.2	112.3
Thrust deduction (t)		0.406	0.294	0.251
K_{QOM}		0.0335	0.0295	0.0285
J		0.78	0.78	0.779

J_{TM}		0.5	0.58	0.59
W_{TM}		0.358	0.257	0.243
Open water efficiency (η_{OTM})		0.5226	0.58	0.576
Hull efficiency (η_{HM})		0.926	0.95	0.9895
Rotative efficiency (η_{RT})		0.988	0.95	0.946
Propulsive efficiency (η_D)		0.478	0.526	0.54

* Values determined based on thrust identity

10.3 Analysis

Table 33: Comparison with reference to the initial propeller location of case1

	Pr1/Pos0	Pr1/Pos1	Pr1/Pos2	Pr2/Pos0	Pr2/Pos1	Pr2/Pos2
Open water efficiency η_{OTM}	Ref	6.15	7.16	2.7	14.5	13.3
Hull efficiency (η_{HM})	Ref	5.97	8.55	-7.3	-4.89	-0.89
Rotative efficiency (η_{RT})	Ref	-3.17	-3.43	-0.45	-4.13	-4.6
Propulsive efficiency (η_D)	Ref	8.92	12.34	-5.18	4.41	7.07
Delivered Power (Watts)	Ref	-8.19	-10.98	5.5	-4.22	-6.59

*Ref- Reference *Pr1- Original propeller, Pr2- Large area propeller, Pos- Position.

*Variation calculated as $-\left(\frac{Ref-Com}{Ref}\right) \times 100$ where Ref is the reference value and Com is the value compared.

10.3.1 Thrust deduction and wake fraction

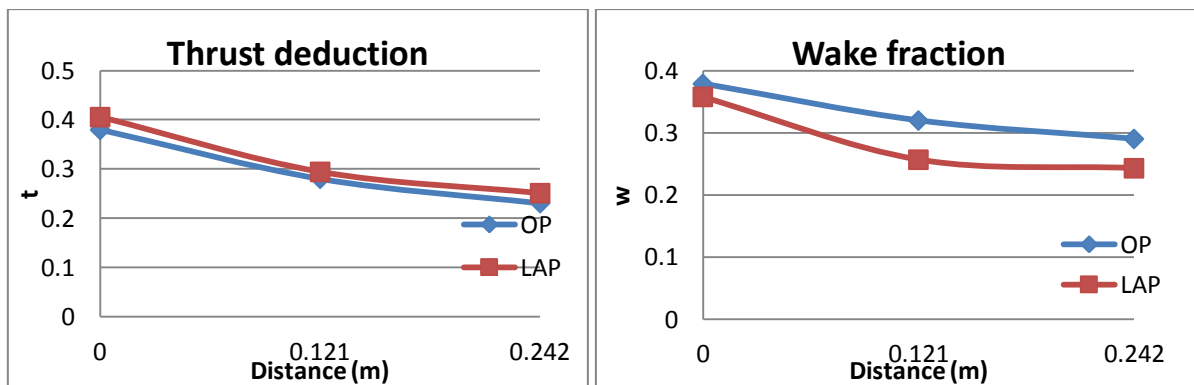


Figure 43: Fig (L) Position vs Thrust deduction, (Fig R) Position vs Wake fraction

The thrust deduction factor t drops rapidly when moving the propeller aft from its original position. The development of thrust deduction versus distance is very small for both the propellers. The wake fraction also shows the same behavior.

10.3.2 Hull efficiency and total resistance

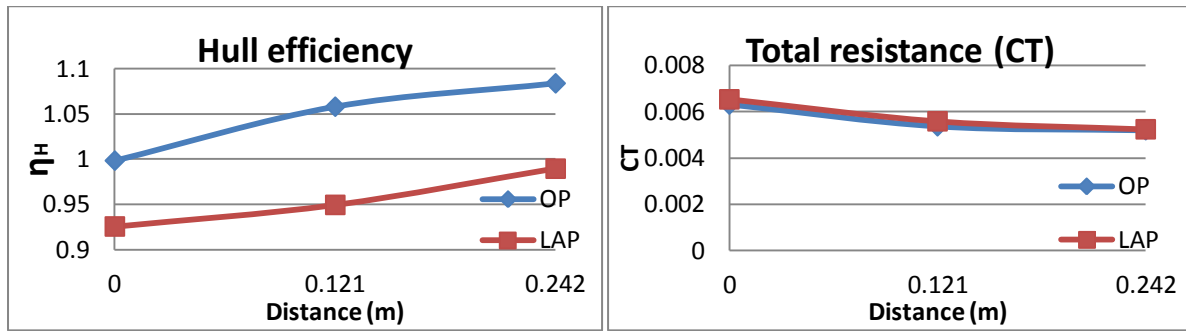


Figure 44: (Fig L) Position vs Hull efficiency, (Fig R) Position vs Total resistance

Hull efficiency is higher with both the propellers for the whole range. To illustrate the physics behind development of hull efficiency, the axial velocity at a cut just in front of the propeller plane is shown for two positions in figure 46 and 47 and the pressure distribution on the aft part of the hull is also shown in figure 45 for propeller1 (propeller2 behavior was similar).

As shown the pressure on the hull increases when moving the propeller aft. When a propeller operates closer to the hull it increases the flow velocity in front of the propeller disc and thereby reduces the pressure on the hull. This is the main cause of thrust deduction and as a result of this there is also an increased friction.

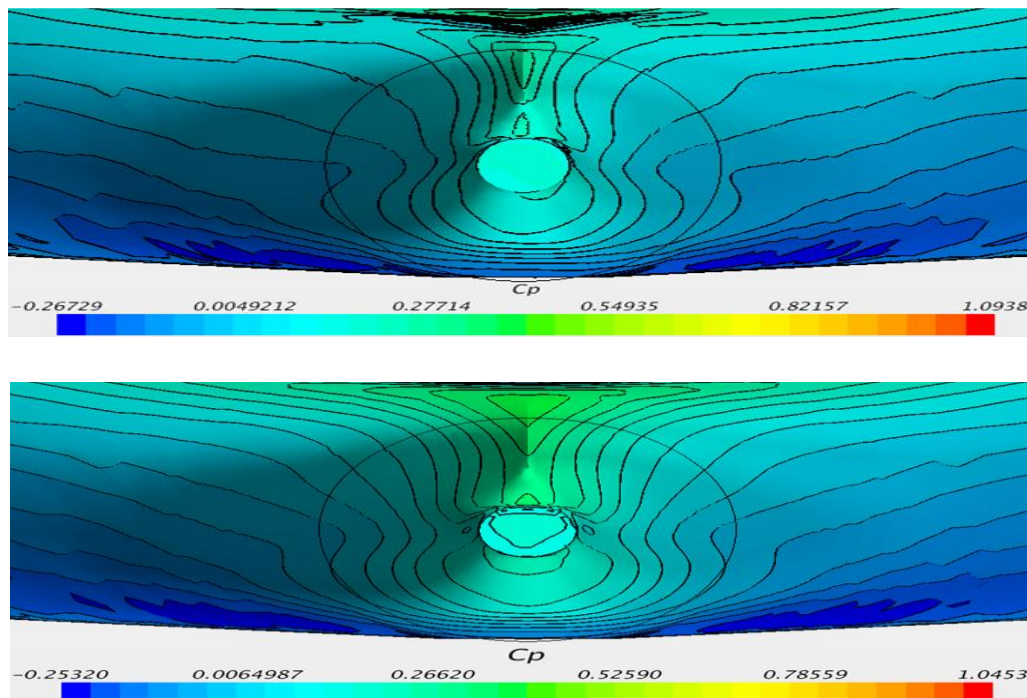


Figure 45: Pressure on the hull (Top) Position 0 (Bottom) Position 2.

When propeller operates away from the hull the flow velocity increases and it operates closer to the free stream velocity when moving the propeller aft. Velocity is measured with a line probe just upstream of the propeller in the transverse axis at a distance corresponding to the centre of propeller from the keel (velocity opposite to ships motion hence -). Figure 47 shows an increase of velocity with position 2 for the chosen propeller. Similar trend was observed for both the propellers [negative sign (-) implies velocity downstream of propeller according to the chosen axis].

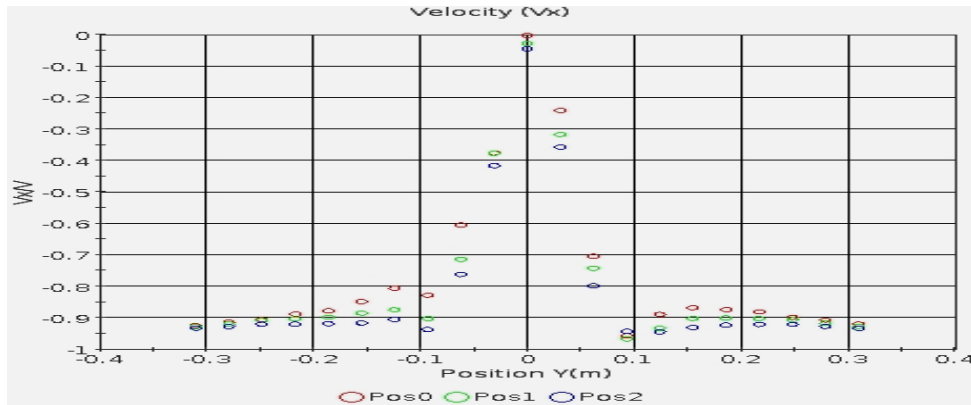


Figure 46: Velocity just upstream of the propeller in a line along y axis.

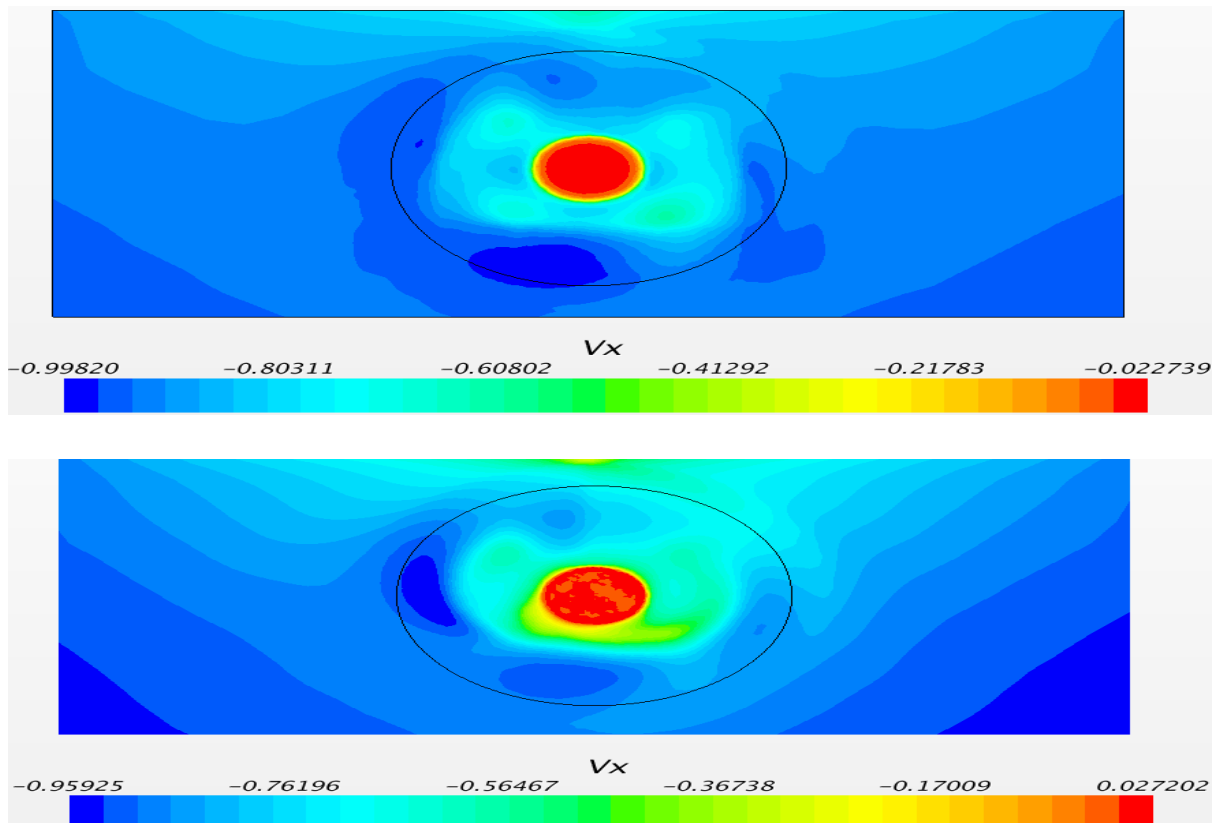


Figure 47: Velocity profile just upstream of the propeller plane (T) Pos 2, (B) Pos 0

10.3.3 Rotative and open water efficiency

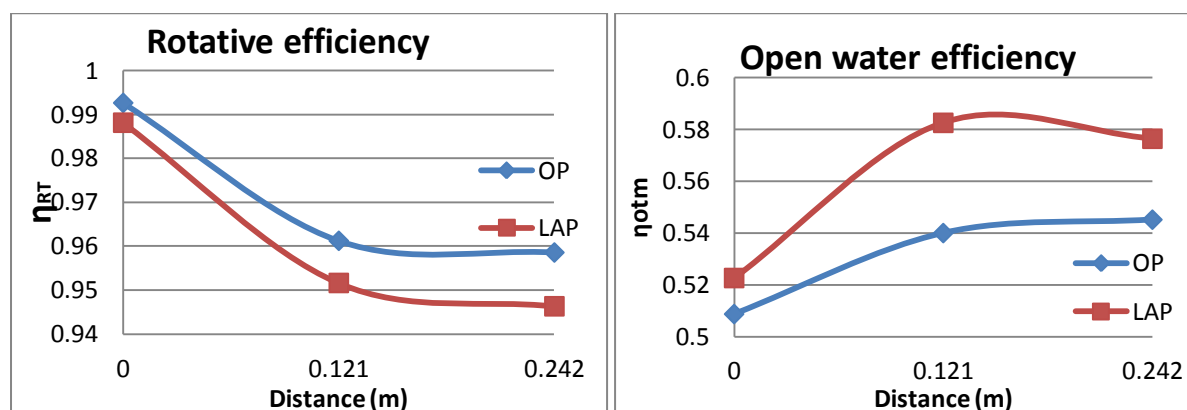


Figure 48: Position vs Rotative efficiency (L), Position vs open water efficiency (R)

The figure shows that for the original position the rotative efficiency is higher for both the propellers where the wake is non homogeneous. It decreases with distance from the hull. In the uneven wake flow the drag of the propeller sections is reduced due to Katzmayr [2] effect which results in a reduction of K_Q for a given K_T . Another reason is that the propeller is wake adapted i.e., designed for the hull wake. They may thus be less efficient in a homogeneous inflow.

The propeller open water efficiency is shown for both propellers and positions. Propeller2 shows a significantly higher larger efficiency and this really shows the main reason for choosing the large area propellers for ships. It has to be noted that both propellers operate close to optimum working point.

The extraction [15] [2] of energy from unsteady flows using a stationary foil is called the Katzmayr effect, after the German engineer who first studied it in 1922. He did experiments in the wind tunnel by mounting an airfoil in the open test section while subjecting the air stream to periodic oscillations. The effect of flowing air whose direction is undergoing periodic constant changes yielded favourable results ([15] "Effect of the periodic changes of angle of attack on behavior of airfoils"). Based on this In 1991 an experiment done by Michael et al., George et al. by placing a flapping foil some distance behind a cylinder in stream. Rows of vortices generated by the cylinder moved toward the foil, which could pitch and moved sideways to encounter them in various positions. Systematic experiments confirmed that these adjustments could enhance or decrease efficiency. When the timing was right vortices created by foil oscillations met incoming vortices spinning in the opposite direction. This effect weakened the vortices in the wake resulting in the capture of energy by the foil and an increase in its efficiency.

10.3.4 Propulsive efficiency and delivered power

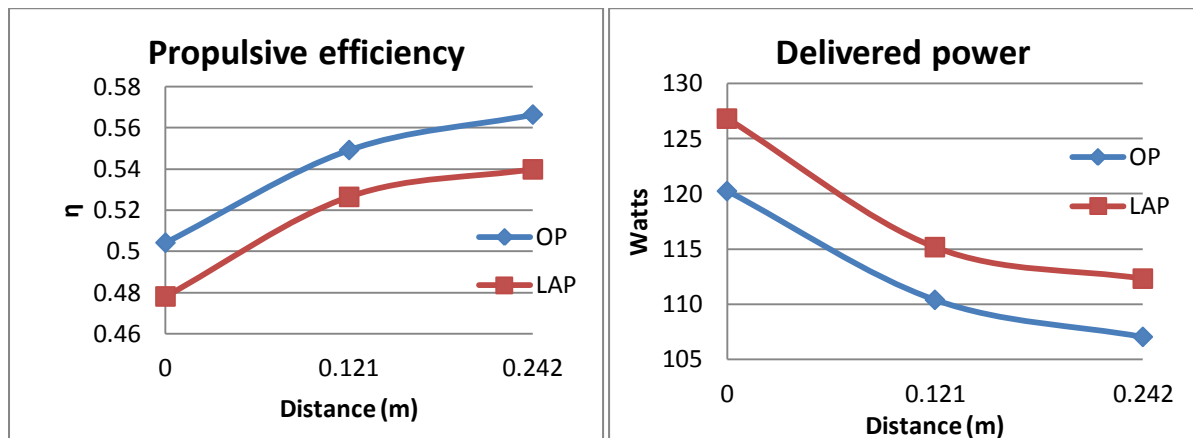


Figure 49: Position vs Propulsive efficiency (L) Position vs Delivered power (R)

Having analyzed all contributions to the final efficiency the figure shows the variation of the total efficiency. The reason for the increase of efficiency is the open water and hull efficiency which increases more than the decrease in relative rotative efficiency

The minimum delivered power is obtained for Pos2 for both the propellers. Also a very interesting trend is noticed here even when the propeller is moved a few distance away from its original position there is 8% decrease of delivered power for the original propeller.

Table 34: Delivered power comparison with positions.

	Pr1/Pos0	Pr1/Pos1	Pr1/Pos2	Pr2/Pos0	Pr2/Pos1	Pr2/Pos2
Delivered Power variation (%)	Reference	-8.19	-11.0	5.5	-4.22	-6.59

Pr1- Propeller1, Pr2- Propeller2, Pos 0- Position 1, Pos2- Position 2 respectively.

10.3.5 Velocity vector

A plane just upstream of the propeller plane is chosen to study the vortices which is an important parameter for vibrations and it is observed being reduced while moving the propeller aft.

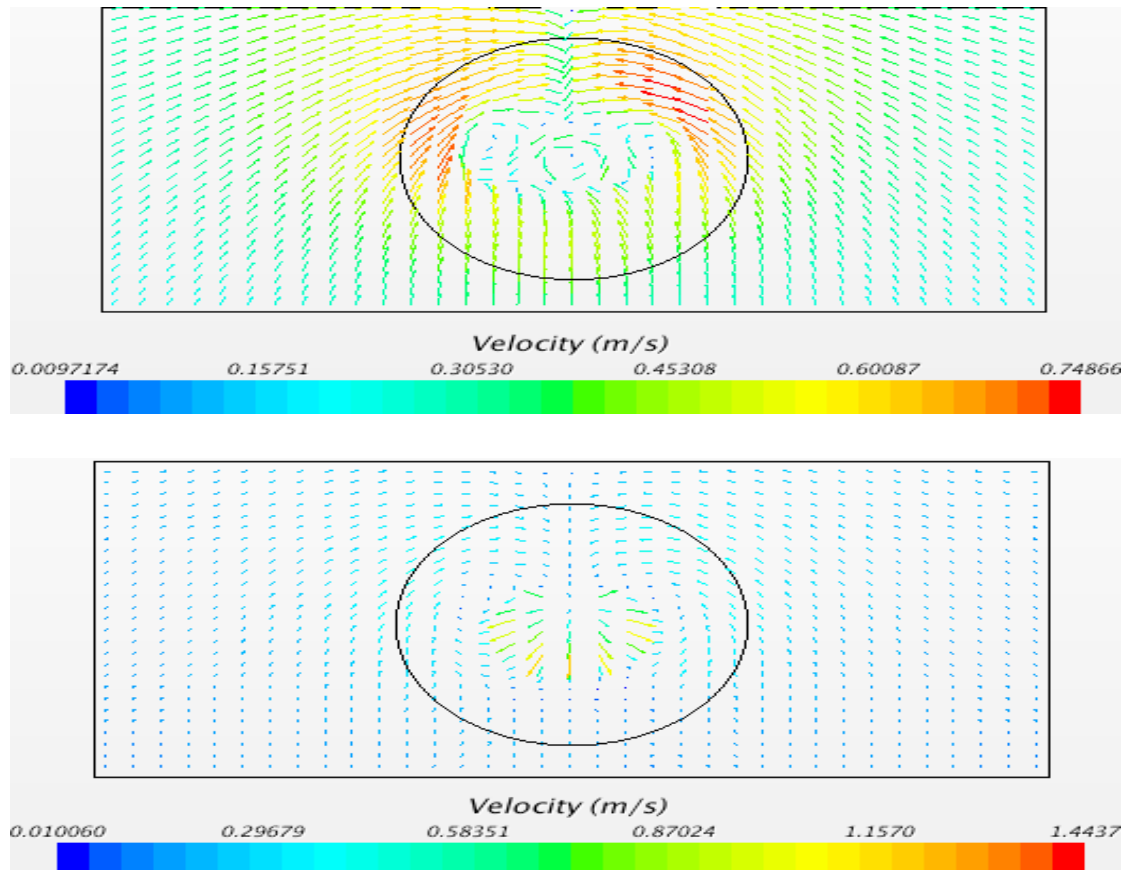


Figure 50: Velocity vector just upstream of propeller1 plane (Top) Position 0 (Bottom) Position 2

11 APPLICATION

The analyzed vessel in the master thesis is a research vessel and it is not included in the EEDI formulation by IMO. Nevertheless a percentage of savings (value obtained for propeller position is chosen for analysis) in power reduction attained in model scale (full scale prediction yielded unrealistic results which needs further investigation) is analyzed against its influence on the EEDI factor of a bulk carrier and the results are as follows:

(It is not a straight forward comparison, it is demonstrated to show the influence of power savings in percentage with respect to the EEDI value):

Vessel considered: Bulk carrier, MCR Main engine: 6900 kw, DWT- 55000 Tons, Ref. Speed: 4.25 Knots. (page 34)

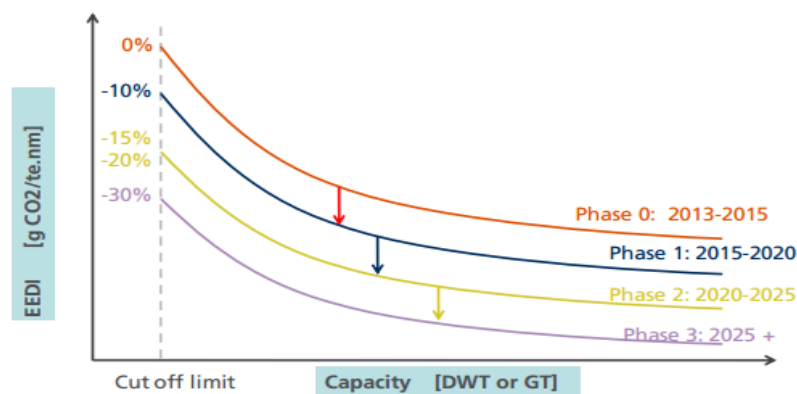


Figure 51: EEDI reduction in various phases

$$\text{Attained EEDI} = \frac{(6900 \times 3.206 \times 171) + (381 \times 3.206 \times 205)}{(1.017 \times 55000 \times 14.25)} = 5.06 \text{ g/ t.nm}$$

Table 35: EEDI analysis for the results

Attained EEDI	Required EEDI (Phase 0)	Required EEDI (Phase 1)	Result
5.06 g/t.nm	5.27 g/t.nm	4.74 g/t.nm (10% margin reduced)	Valid in phase 0 but for phase 1
Delivered power gain of 8.2% resulted in 4.66 g/t.nm			Phase 1 requirement satisfied

12 CONCLUSION

- Moving the propeller aft indicated some interesting trends in the propulsion factors. Even though the delivered power of the large area propeller can't be reduced more than the default propeller the trends have been analyzed and based on this an optimum propeller with appropriate Pitch/ Diameter (P/D) ratio can be chosen in future.
- When the propeller moved aft there is a very good trend of decrease in delivered power. The reason for the increase of efficiency in this experiments are the open water and hull efficiency which increased more than the decrease in relative rotative efficiency. While moving the propeller aft the clearance also increased for the propellers considered. This can result in a reduction of pressure pulses which is most crucial for vibration and fatigue problem if it moved slightly away from the hull as done by [Knutsson et al.](#)
- The series of experiments demonstrated the applicability of Realizable K- ϵ models which proved effective for this type of calculations.
- The influence of mesh size and the critical mesh refining techniques were studied.
- It also demonstrated the effectiveness of Star-CCM+ for this kind of flow simulations.
- This investigation was carried out without rudder and optimization methods. Hence if we consider them we can achieve even more greater reduction of power.
- It can be concluded that if appropriate large area propeller is fixed in appropriate location behind the ship significant amount of power savings can be realized which is the key factor to satisfy the more stringent EEDI phases in future.

13 FUTURE WORK

The work can be continued by choosing the optimum P/D ratio as demonstrated in the experiments done by the leading propulsion engine manufacturer MAN-B&W (1) and in a research work done at Chalmers University (Knutsson et al) with large area propellers which resulted in considerable delivered power reduction as in figure: 51.

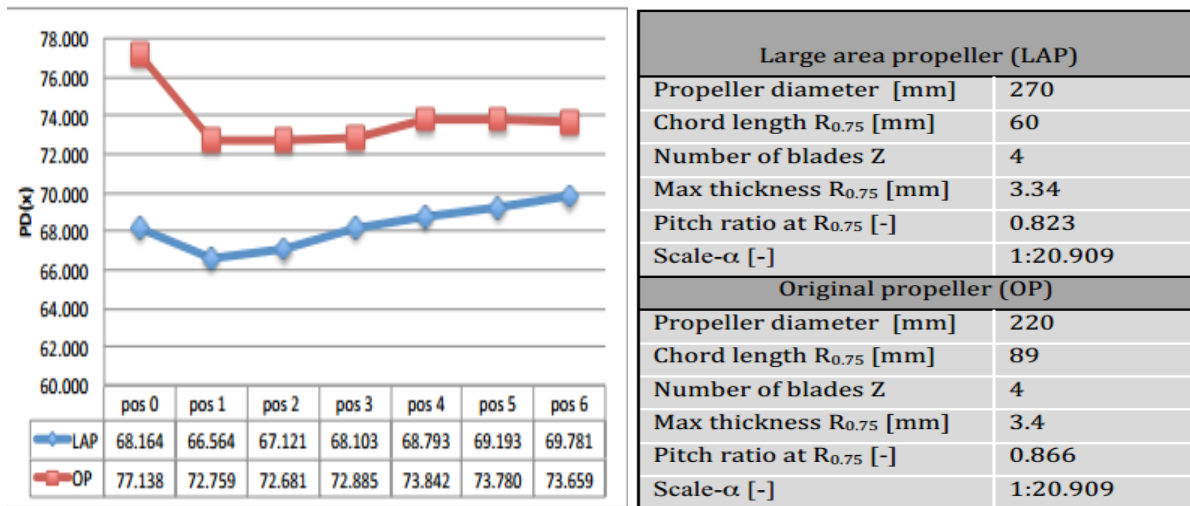


Figure 52: Variation of delivered power when propeller moved aft (42).

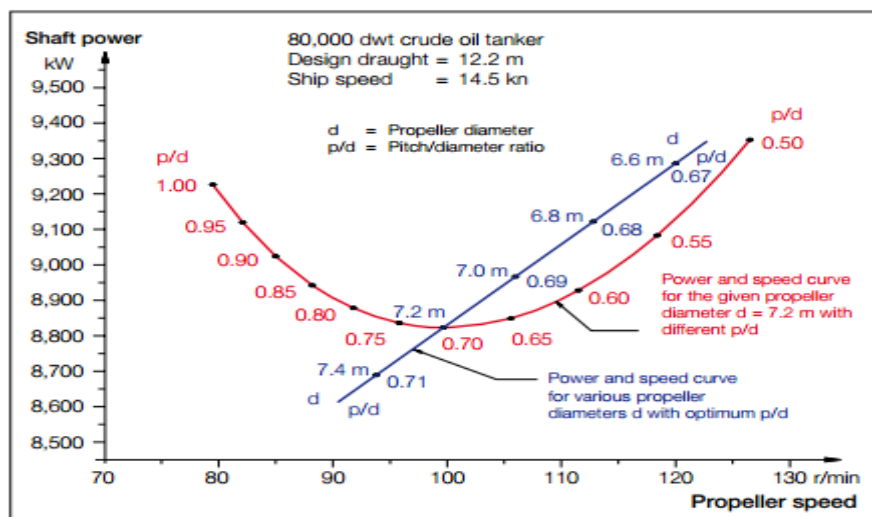


Figure 53: Influence of P/D ratio in propeller design (42)

14 ACKNOWLEDGEMENTS

I would like to acknowledge everyone who have helped me during the EMSHIP study program which enabled me a great learning experience.

First of all I would like to thank Prof. Phillipe Rigo from University of Liege (ULG) as a coordinator of the EMSHIP program along with Prof. Pierre Ferrant from Ecole Centrale de Nantes (ECN) and Prof. Maciej Taczala from West Pomeranian University of Technology (ZUT), Szczecin as local coordinators of EMSHIP program in France and Poland. I thank them for their technical guidance, help on academic and administrative issues.

I would like to mention that I would be grateful for the guidance and feedback from Prof. Zbigniew Seluski from ZUT as my master thesis supervisor. His advices were very helpful to improve the work presented in this master thesis.

As this master thesis was mainly developed at Ship Design and Research Centre (CTO S.A.), I would like to convey my sincere regards to Dr. Wojciech Górski, Head of the hydromechanics division for giving me an opportunity to pursue this internship. During the stay of four months my colleagues were very supportive and make me feel a part of the organization. My special thanks to Dr. Sebastian Kowalczyk for organizing the internship in a structured manner which enabled me to achieve my goal. I would like to thank Dr. Tomasz Bugalski and Mr. Pawel Hoffmann specially for sharing their practical insight and great patience which helped me for completing my work successfully.

Finally I would like to thank my family and friends for their support which made these eighteen months a memorable part in my life.

This thesis was developed in the frame of the European Master Course in “Integrated Advanced Ship Design” named “EMSHIP” for “European Education in Advanced Ship Design”, Ref.: 159652-1-2009-1-BE-ERA MUNDUS-EMMC.

15 REFERENCES

15.1 Publications

- [1] *Third IMO GHG Study 2014*, International Maritime Organization (IMO), July 2014
- [2] *Second IMO GHG Study 2009*, International Maritime Organization (IMO) London, UK, April 2009; Buhaug, Ø., Corbett, J.J., Endresen, Ø., Eyring, V., Faber, J., Hanayama, S., Lee, D.S., Lee, D., Lindstad, H., Markowska, A.Z., Mjelde, A., Nelissen, D., Nilsen, J., Pålsson, C., Winebrake, J.J., Wu, W., Yoshida, K.
- [3] IPCC, 2007: Climate Change 2007: Synthesis Report. Contribution of Working Groups I, II and III to the Fourth Assessment Report of the Intergovernmental Panel on Climate Change [Core Writing Team, Pachauri, R.K and Reisinger, A.(eds.)]. IPCC, Geneva, Switzerland, 104 pp.
- [4] United States Environmental Protection Agency (EPA) report. <http://www.epa.gov/climatechange/ghgemissions/gases/co2.html>
- [5] Heitmann, Nadine, and Setareh Khalilian. "Accounting for carbon dioxide emissions from international shipping: Burden sharing under different UNFCCC allocation options and regime scenarios." *Marine Policy* 35.5 (2011): 682-691.
- [6] History and status of GHG Emissions control in International shipping, G. Reynolds, GL Reynolds consultants, UK. http://www.lowcarbonshipping.co.uk/files/ucl_admin/LCS%202011/THE_HISTORY_AND_STATUS_OF_GHG_EMISSIONS_CONTROL_IN_INTERNATIONAL_SHIPPING.pdf
- [7] Design for Energy Efficiency: Simulation-Driven Design and Hydrodynamic Optimization for Greener Ships and EEDI Compliance, Mattia Brenner, Bekir Şener, 1st International Symposium on Naval Architecture and Maritime (INT-NAM 2011), © October 2011 | Istanbul, Turkey
- [8] Bugalski, Tomasz, and Paweł Hoffmann. "Numerical Simulation of the Self-Propulsion Model Tests." *Proceeding of 2nd International Symposium on Marine Propulsors*. 2011.
- [9] Dhinesh, G., V. Anantha Subramaian, and K. Murali. "SUB DOMAIN BASED NUMERICAL MODELING OF SHIP HULL PROPELLER INTERACTION." (2009).
- [10] Enger, Sven, Milovan Perić, and Robinson Perić. "Simulation of flow around KCS-hull." *A Workshop on Numerical Ship Hydrodynamics*. 2010.
- [11] Knutsson, Daniel, and Lars Larsson. "Large area propellers." *SMP'11 (Symposium on Marine Propulsors)*. 2011.
- [12] CD-adapco, U. S. E. R. "GUIDE Star CCM+ Version 9.02."
- [13] Hirt, Cyril W., and Billy D. Nichols. "Volume of fluid (VOF) method for the dynamics of free boundaries." *Journal of computational physics* 39.1 (1981): 201-225.
- [14] Computation of Free Surface Viscous Flows around self propelled ships with the help of sliding grids, (M. Visonneau, P. Queutey, D. Gan Bo, J. Wackers, E. Guilmineau, A. Leroyer, B. Mallo), COMPIT 2012

[15] Katzmayr, R., Effect of periodic changes of angle of attack on behavior of airfoils, NACA TM 147, October 1922.

[16] Szelangiewicz, T., and K. Żelazny. "Increasing ship propulsion efficiency as an alternative to help reduce fuel consumption and CO₂ emission. Part 2." *Journal of Polish CIMAC* 7 (2012): 235-244.

[17] Ship Energy Efficiency Measures, Status and Guidance: American Bureau of Shipping.

[18] Mørch, H. J., Enger, S., Peric, M. and Schreck, E. (2008). *Simulation of lifeboat launching under storm conditions*, 6th International Conference on CFD in Oil & Gas, Metallurgical and Process Industries, SINTEF/NTNU, Trondheim, Norway, 10-12 June, 2008.

[19] Demirdžić, I., and S. Muzaferija. "Numerical method for coupled fluid flow, heat transfer and stress analysis using unstructured moving meshes with cells of arbitrary topology." *Computer methods in applied mechanics and engineering* 125.1 (1995): 235-255.

R.E. Collison, M.C. James, S.R. Turnock, D.A. Hudson Retro-fit Solutions for Energy Efficient Shipping, Ship Science Report n0:148, Faculty of Engineering and Environment Ship Science, University of Southampton (2013).

Nakisa, Mehdi, Mohammad Javad Abbasi, and Ahmad Mobasher Amini. "Assessment of Marine Propeller Hydrodynamic Performance in Open Water via CFD." *Proceedings of MARTEC, The International Conference on Marine Technology, BUET, Dhaka, Bangladesh*. 2010.

Livanos, George A., Gerasimos Theotokatos, and Dimitrios-Nikolaos Pagonis. "Techno-economic investigation of alternative propulsion plants for Ferries and RoRo ships." *Energy Conversion and Management* 79 (2014): 640-651.

Tsung-Yueh Lin • Jen-Shiang Kouh, On the scale effect of thrust deduction in a judicious self-propulsion procedure for a moderate-speed containership, Department of Engineering science and Ocean Engineering, National Taiwan University, (2014) DOI 10.1007/s00773-014-0289-7, Springer.

15.2 MEPC Guidelines

[20] Resolution mepc.212(63), annex 8, resolution mepc.212(63), adopted on 2 march 2012, 2012 guidelines on the method of calculation of the attained energy efficiency design index (EEDI) for new ships.

[21] MEPC 63/23, Annex9, resolution mepc.213(63), adopted on 2 march 2012, 2012 guidelines for the development of a ship energy efficiency management plan (seemp)

[22] IMO Guidelines for voluntary use of the Ship Energy Efficiency Operational Indicator (EEOI), MEPC.1/Circ.684, 17 August 2009

Annex 5, resolution mepc.245(66), adopted on 4 april 2014, 2014 guidelines on the method of calculation of the attained energy efficiency design index (eedi) for new ships.

MEPC 63/23, Annex 11, resolution mepc.215(63), adopted on 2 march 2012, guidelines for calculation of reference lines for use with the energy efficiency design index (eedi).

MEPC 61/INF.2, reduction Of Ghg Emissions From Ships

15.3 ITTC Procedures

[23] ITTC- Recommended Procedures and Guidelines 7.5-02-02-01, Resistance Test, Revision 03, (2011).

[24] ITTC- Recommended Procedures and Guidelines 7.5-03-02-03, Practical Guidelines for Ship CFD Applications, Revision 01, (2011).

[25] ITTC- Recommended Procedures and Guidelines 7.5-02-03-02.1, Testing and Extrapolation Methods Propulsion, Propulsor Open Water Test, Revision 02, (2008).

[26] ITTC- Recommended Procedures and Guidelines 7.5-02-03-01.1, Testing and extrapolation methods propulsion, performance propulsion test, Revision 01, (2002).

15.4 Master thesis

[27] CFD for Underhood modeling, Emil Ljungskog, ULF Nilsson, Chalmers University of Technology (2014).

[28] Computational modeling of propeller noise NASA SR-7A propeller, Karim Moussa, University of Waterloo (2014).

[29] Kanu Priya Jain, "Impacts of Energy Efficiency Design Index", Newcastle University, (2012).

[30] S.M. Rashidul Hasan, "Impact of EEDI on Ship Design and Hydrodynamics" Department of Shipping and Marine Technology, Chalmers University of Technology (2011).

Rolf Arild Topphol, "The efficiency of a Mewis Duct in Waves", Department of Marine Engineering, Norwegian University of Science and Technology (2013).

Espen Oyan, "Speed and powering prediction for ships based on model testing", Department of Marine Engineering, Norwegian University of Science and Technology (2012).

S.W. Van Haren, "Testing DNS capability of OpenFOAM and Star-CCM+", Delft University of Technology, (2011).

Øyvind Pedersen, "3D Numerical Modelling of Hydropeaking Scenarios in Norwegian Regulated Rivers", Norwegian University of Science and Technology (2012).

15.5 Presentation/ Symposium

[29] Procedure for calculation and verification of the Energy Efficiency Design Index (EEDI), International Association Of Classification Societies Ltd IACS Proc Req. 2013.

[30] Larsson, Lars, Frederick Stern, and Michel Visonneau. "Gothenburg 2010, A Workshop on Numerical Ship Hydrodynamics." (2010).

[31] Implementing EEDI, a guidance for owners, operators, shipyards and tank testing organisations, Lloyd's Register (2012).

- [32] <http://www.ics-shipping.org/docs/default-source/resources/environmental-protection/shipping-world-trade-and-the-reduction-of-co2-emissions.pdf?sfvrsn=4>
- [33] Lecture slides Prof. Lionel Gentaz, Prof. David Le Touze, Prof. Pierre Ferrant.
- [34] Lecture notes, Physical oceanography, Prof. P. Ananthkrishnan.
- [35] Prof. Gautam Biswas IIT Kanpur, Computational Fluid Dynamics and Heat Transfer (Web) <http://nptel.ac.in/courses/112104030/>
- [36] Use of CFD in Design: A Tutorial, Sean M. McGuffie, P.E, Michael A. Porter, P.E, Thomas T. Hirst.
- [37] <http://www.cd-adapco.com/products/star-ccm%C2%AE/motion>
- [38] Historic background of emission regulations, IMO.
<http://www.imo.org/OurWork/Environment/PollutionPrevention/AirPollution/Pages/Historic%20Background%20GHG.aspx>
- [39] Multi physics simulation for marine application, CD-adapco, Milovan Peric,
<http://www.cd-adapco.com/presentation/multiphysics-simulation-marine-applications>
- [40] Fluid Dynamics: Theory and Computation Henningson, Dan S. "Martin Berggren August 24, 2005." (2005).
- [41] Retrofit- Propulsion improvement, Wartsila-Propulsion Services.
<http://www.wartsila.com/en/propulsion-services-products/propulsion-improvement>.
- [42] Basic Principles of Ship Propulsion, MAN Diesel & Turbo.
<http://marine.man.eu/docs/librariesprovider6/propeller-aftship/basic-principles-of-propulsion.pdf?sfvrsn=0>
- [43] Energy Efficiency Design Index MAN Diesel & Turbo.
EEDI <http://www.mandieselturbo.us.com/files/news/files/7791/eedi.pdf>
- [44] Fathom FOCUS- Hull coatings for vessel performance
<http://fathomshipping.com/userfiles/files/b85b16066a682bcef16114f6b63c65b2.pdf>
- 17th Numerical Towing Tank Symposium (NuTTS'14) Marstrand, Sweden, 28-30 September 2014 https://www.uni-due.de/imperia/md/content/ist/nutts_17_2014_marstrand.pdf
- CFD under viscous flow theory: Velocity-Pressure coupling, Dr. Lionel Gentaz, Ecole Centrale De Nantes
- <http://site.rightship.com/ship-owners/environmental-ratings>
RightShip's EVDI™ and GHG Emissions Rating.

15.6 Literature

- [45] Ghose, J. P., and R. P. Gokarn. *Basic ship propulsion*. Allied Publishers, 2004.
- [46] Ferziger, Joel H., and Milovan Perić. *Computational methods for fluid dynamics*. Vol. 3. Berlin: Springer, 2002.
- [47] Bertram, Volker. *Practical ship hydrodynamics*. Elsevier, 2012.